JOURNAL OF GEOPHYSICAL RESEARCH, VOL. 101, NO. C2, PAGES 3435–3455, FEBRUARY 15, 1996

The fate of river discharge on the continental shelf 2. Transport of coastal low-salinity waters under realistic wind and tidal forcing

Vassiliki H. Kourafalou[1] and Thomas N. Lee

Rosenstiel School of Marine and Atmospheric Science, University of Miami, Miami, Florida

Lie-Yauw Oey

Atmospheric and Oceanic Science Program, Princeton University, Princeton, New Jersey

John D. Wang

Rosenstiel School of Marine and Atmospheric Science, University of Miami, Miami, Florida

Abstract. A three-dimensional numerical simulation of shelf circulation is presented. We employ realistic forcing for the Southeast U.S. Continental Shelf during the spring season. We show that the strongest offshore transport of river-induced, coastal, low-salinity waters and associated materials occurs near the surface. The preferred mean pathway is in the northeastward direction, and it takes about 2 months to cross the entire shelf. Owing to the mean direction of surface transport and the topography of the South Atlantic Bight shelf, the preferred location for springtime removal is off Charleston, South Carolina, and presumably in the vicinity of the Charleston Bump. The transport and fate of the river-induced, coastal, low-salinity waters during the spring season are determined by (1) the stratification of nearshore waters, which is due to the high river runoff and causes the decoupling between "near-surface" and "near-bottom" layers; (2) the prevailing northeastward winds, which cause significant offshore transport within the shallow near-surface Ekman layer; and (3) the tidally induced bottom stirring (M_2 tides). Comparison of model and data time series of currents shows very good agreement. Standard deviations of the model and data-computed empirical orthogonal functions are almost identical, while the respective variance-conserving spectra agree both in amplitude and phase.

1. Introduction

We study the part of the continental margin that extends from approximately West Palm Beach, Florida, to Cape Hatteras, North Carolina (Figure 1). This is the "Southeast U.S. Continental Shelf" (South Atlantic Bight (SAB)), and it can be divided into the following three regions: inner shelf (from the coast to the 20-m isobath), midshelf (depths between 20 and 40 m) and outer shelf (from the 40-m isobath to the shelf break, generally defined at the 75-m isobath). The important forcing mechanisms for SAB flow are the wind, tides, coastal runoff, and the interaction with the deep oceanic flow, which is mainly controlled by the Gulf Stream.

The motivation of the present study arose from the interest in understanding the circulation processes that govern the exchange of materials between the continental shelf and the adjacent ocean. We use the word "materials" to refer to all conservative and nonconservative trace elements, nutrients, sediments, radionuclides, and pollutants in general. The major portion of materials enters the SAB nearshore waters through river discharge. Twelve major rivers provide the freshwater input along the coast (Figure 1), forming a nearshore band of low-salinity water [*Atkinson et al.*, 1983]. The ability to predict the path of this water is essential for assessing the dispersal of materials. Therefore our objective is to quantify the processes that influence the transport of the nearshore low-salinity waters on the continental shelf.

On the basis of data, *Blanton and Atkinson* [1983] concluded that the river-runoff-generated, low-salinity water is carried offshore in spring and alongshore and southward in autumn. The low-salinity water appeared to end up near the shelf break around 32°N to 34°N in spring and off northern and central Florida in autumn. The above qualitative results were based on the seasonal cycle of river runoff and wind stress: maximum runoff and upwelling-favorable winds in the spring season, low runoff and downwelling-favorable winds in the fall. The role of wind stress and shelf geometry/bathymetry in guiding the springtime transport on the SAB was elaborated in the numerical study of *Kourafalou et al.* [1984]. A one-layer

[1] Now at Consiglio Nazionale delle Ricerche, Istituto per lo Studio delle Metodologie Geofisiche Ambientali, Modena, Italy.

Paper number 95JC03025.
0148-0227/96/95JC-03025$05.00

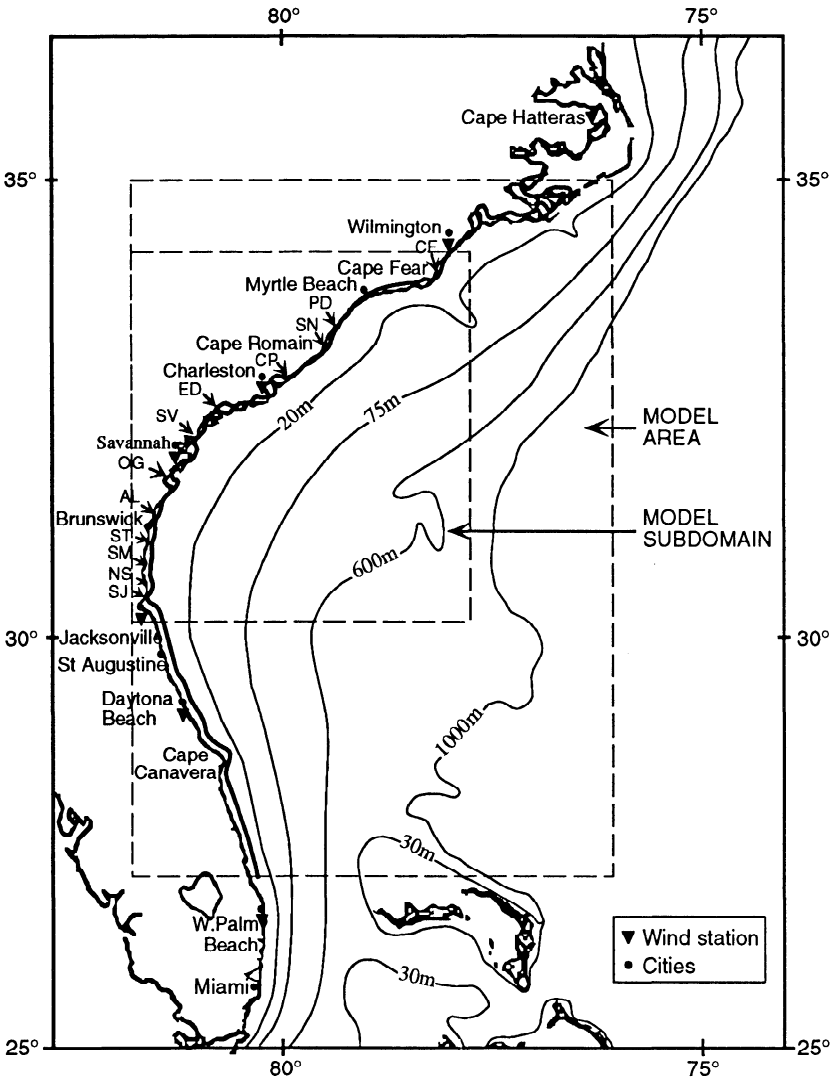

Figure 1. The Southeast U.S. Continental Shelf, the numerical model area, and a model subdomain used for the presentation of results.

finite element hydrodynamic model [*Wang and Connor*, 1975] was adopted to simulate the vertically integrated flow on the SAB during upwelling-favorable winds. Although the model gave good insight into the general circulation pattern, the grid did not resolve the inner shelf in detail and the numerical simulation was too brief to determine the rate of springtime transport. Furthermore, since density was not included as a variable, the dynamical role of stratification due to freshwater discharge was neglected.

Previous studies on the interaction of buoyancy and wind forcing in the SAB were mainly based on analysis of data and are reviewed by *Kourafalou et al.* [this issue] (hereinafter referred to as part 1). In part 1 we performed three-dimensional numerical process studies on the SAB; we included realistic bathymetry and a 5 km by 5 km horizontal grid. We concluded that the development and evolution of a river plume (or of a river-induced, coastal, low-salinity band) are governed by the dynamics of the inner shelf and the seasonal forcing conditions. We showed that the buoyancy-driven southward baroclinic coastal current would be enhanced during downwelling-favorable wind conditions (typical of the fall season), while opposed and frequently reversed during upwelling-favorable wind conditions (typical during spring). We inferred that the strongest offshore transport of riverine waters (and therefore transport of associated materials) would be expected in springtime. Part 2 deals with a realistic simulation of flow and transport on the SAB during the spring of 1984. The particular year was chosen for having "typical" springtime conditions and for the availability of measurements during the pre-Spring Removal Experiment (pre-SPREX) field study, which included moored current meters and hydrographic sections.

The three-dimensional (3-D) numerical simulation includes freshwater runoff, wind stress, and tides. We compare model results with measurements. The interaction of the continental shelf with the adjacent Gulf Stream is ignored, since the study concentrates on the shallow regions of the continental shelf. We also neglect heat and moisture fluxes and temperature variations. Thus wind stress is considered as the primary surface forcing, while the density variability is due to salinity changes.

Table 1. Specified Tidal Amplitude and Phase Along the Eastern and Southern Open Model Boundaries

Latitude, deg	Amplitude, cm	Phase, deg
	Eastern Boundary	
35	45	355
34	46	357
33	46	358
32	44	1
31	42	2
30	41	5
29	40	7
28	36	10
	Southern Boundary	
76	36	11
77	38	9
78	38	10
79	42	12
80	40	16

Values are Adopted from *Schwiderski*, [1980]

2. The Model

2.1. The 3-D Hydrodynamic Model

We use a modified version of the *Blumberg and Mellor* [1983] model, presented by *Oey and Chen* [1992]. The model domain is shown in Figure 1. We specify minimum coastal depth at 2 m and maximum ocean depth at 1000 m. A brief presentation of the model and the modifications developed for our adaptation is given in part 1. Here (part 2) the "ß plane approximation" is used and the open ocean boundary condition includes the M_2 tide. A model subdomain that will be used in the presentation of results is also marked in Figure 1.

2.2 SAB Tidal Model

A review of studies on the SAB tidal regime is given by *Pietrafesa et al.* [1985]. It was suggested that tidal currents (dominated by the M_2 component) contribute significantly toward the total kinetic energy of the SAB shelf currents, particularly in the nearshore region. *Kourafalou et al.* [1983] successfully modeled tidal currents on the SAB, and the importance of the M_2 tide on the shelf circulation was verified with both model results and observations. Their model was two-dimensional (vertically integrated) and was forced by tidal elevations from *Scwhwiderski's* [1980] global model, imposed on the boundary condition at the shelf break. Details of the model adaptation and numerical simulation are given by *Wang et al.* [1984]. A similar forcing strategy was followed in this study, using a two-dimensional version (vertically integrated) of the present model. Since the model domain extends much farther offshore than in the work by *Kourafalou et al.* [1983], the global model's output (M_2 amplitude and phase on a 1° by 1° grid) was suitably interpolated for the new open boundaries. The SAB model locations that correspond to the global model grid and the specified tidal forcing at the "east" and "south" open ocean boundaries are given in Table 1.

The main purpose of the present tidal model is to introduce the mixing effect of tides in the calculation of modeled fields. We derived an open ocean boundary condition that includes realistic M_2 tidal forcing. Our approach is similar to *Oey and Chen's* [1992] and is based on an iterative radiation condition at the open boundary, originally developed by *Flather* [1976]. Figure 2 shows the computed tidal elevations during the final days of the integration at four coastal locations. The solution has "converged," and the model-predicted values agree with the observed mean ranges.

The boundary velocity and elevation that were calculated through the two-dimensional "tidal model" were applied to the external velocity open boundary condition during the three-dimensional model calculations as described by *Oey and Chen* [1992]. A process study by *Kourafalou* [1993] verified that the model's parameterization of vertical mixing was, indeed, more realistic when the M_2 tides were included.

3. Modeling Circulation on the SAB During the Spring of 1984

3.1. The Input Data

3.1.1. River discharge. The 12 major rivers in the SAB are presented in Figure 3. The long arrows mark the strongest rivers, with characteristic springtime runoff close to 1000 $m^3\ s^{-1}$. The rivers are modeled as sources of freshwater in the continuity equation [*Kourafalou et al.*, this issue], and the coastal runoff is specified as realistically as possible. The daily values of the combined discharge from the 12 major SAB rivers show that the highest values were around March 10 and April 5 (Figure 4). The first peak was mostly pronounced at the south of SAB rivers (which include the Savannah River and all rivers south of it), while the second peak was mainly due to rivers north of the Savannah River.

3.1.2. Wind data. Wind measurements from the following coastal land stations (Figure 1) were obtained for the model period: West Palm Beach, Daytona Beach, and Jacksonville, Florida; Savannah, Georgia; Charleston, South Carolina; and Wilmington and Cape Hatteras, North Carolina. However, wind measurements from land stations underestimate the magnitude of wind above water surfaces. This is mainly due to differences in the characteristics of the atmospheric planetary boundary layer over land and over water. On the basis of theory discussed by *Hsu* [1981] and comparison of coastal and offshore wind measurements in the SAB during several study periods, *Kourafalou* [1993] proposed the following regression formula for SAB winds (in units of meters per second):

$$U_{sea} = 1.1 + 1.6U_{land} \quad (1)$$

which gives the magnitude of wind above the water U_{sea}, when a coastal measurement U_{land} is available. A clockwise shift in wind direction was also suggested:

$$\Delta\vartheta_{SAB} = 20^0 \quad (2)$$

The above formulas were evaluated by comparing the only offshore wind measurements that were available during the

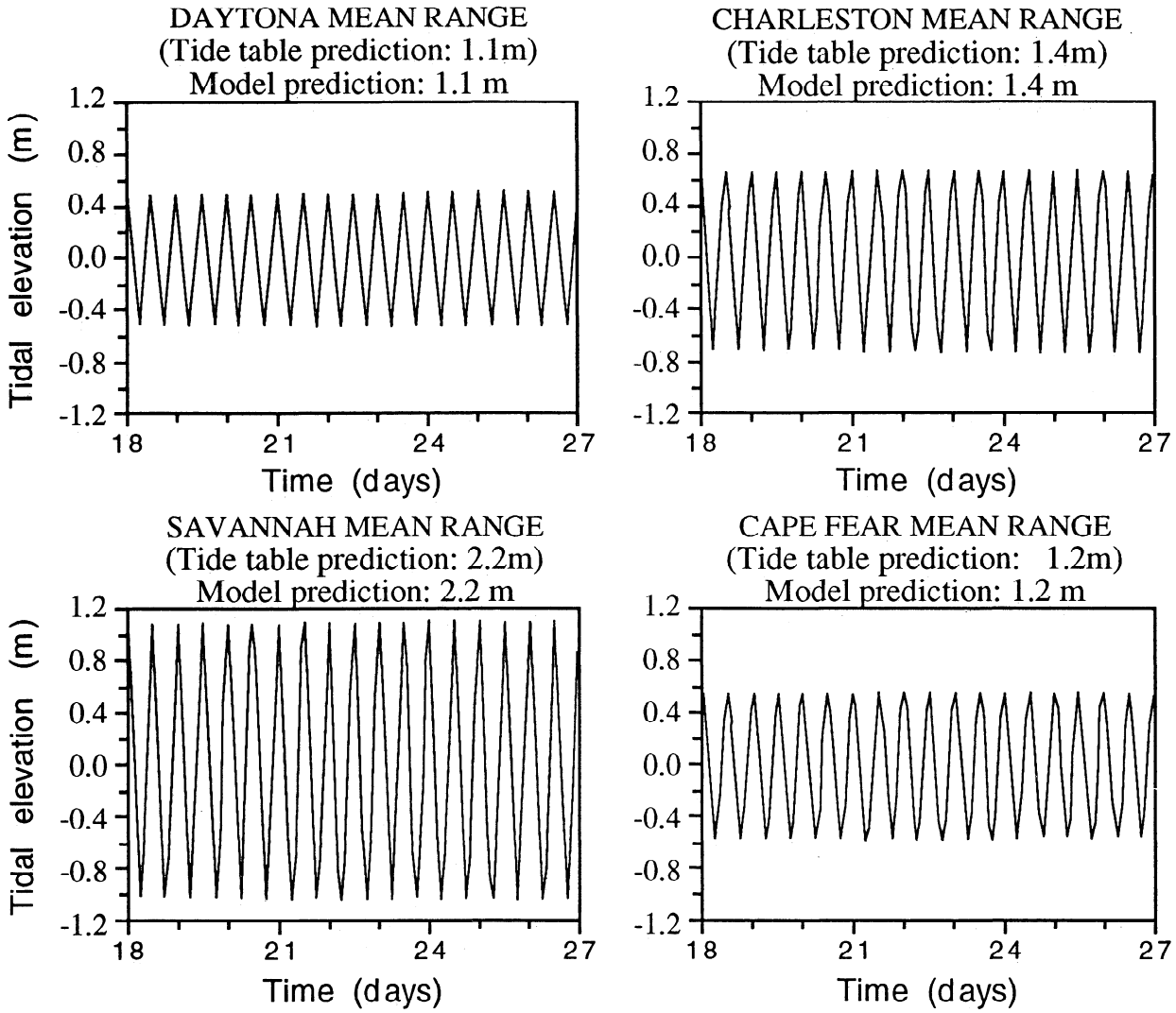

Figure 2. Model-computed tidal ranges at four coastal locations during the last 9 days of the tidal run. Location names and the ranges that are predicted from tide tables are given at the top for comparison.

pre-SPREX study (Savannah Light Tower) to the corresponding coastal wind record (Savannah, Georgia). The agreement between the observed and calculated ocean winds was excellent in both magnitude and direction [*Kourafalou*, 1993].

Bulk methods for estimating wind stress τ_w express it as a function of the wind speed U_z (measured at height z):

$$\tau_w = \rho C_D U_z^2 \tag{3}$$

where ρ is the density of air and C_D is the wind stress drag coefficient. The height that is most commonly taken as a standard reference height for U_z is 10 m. Since the anemometers at the measuring stations can be at any height, we corrected the wind data to the 10 m level. The derivation of the relationship between U_z and U_{10} is given by *Kourafalou* [1993, Appendix C] and is expressed as

$$U_{10} = U_z \left\langle \frac{10}{z} \right\rangle^{0.1}. \tag{4}$$

The estimate of C_D above water depends on the air-sea interaction dynamics considered (such as atmospheric stability and wave development) and on the magnitude range of the wind speed. For reference, the formulas proposed by *Wang* [1978], *Large and Pond* [1981], *Wu* [1982], and *Hsu* [1986] are cited and examples of drag coefficient profiles for different wind speeds are shown by *Kourafalou* [1993]. For the range of wind speeds that enter the present study and with the assumption of neutral atmospheric stability, the following formula was adopted [*Large and Pond*, 1981]:

$$\begin{aligned} C_D &= 1.4\text{x}10^{-3} && 4 \le U_{10} < 10\ m\ s^{-1} \\ C_D &= (0.49 + 0.065U_{10})\text{x}10^{-3} && 10 \le U_{10} < 26\ m\ s^{-1} \end{aligned} \tag{5}$$

The above derivation was applied on the wind measurements from the seven coastal SAB stations, and time series of "ocean" wind stress were composed. The computed values were then interpolated for each horizontal model grid node, taking into account the distance and hence the "weight" of each station from the nodal point. An example of pre-SPREX wind model input that was assimilated in the above manner is given in Figure 5 for shelf areas offshore the specified coastal locations. The presented fields are the product of transformation of coastal

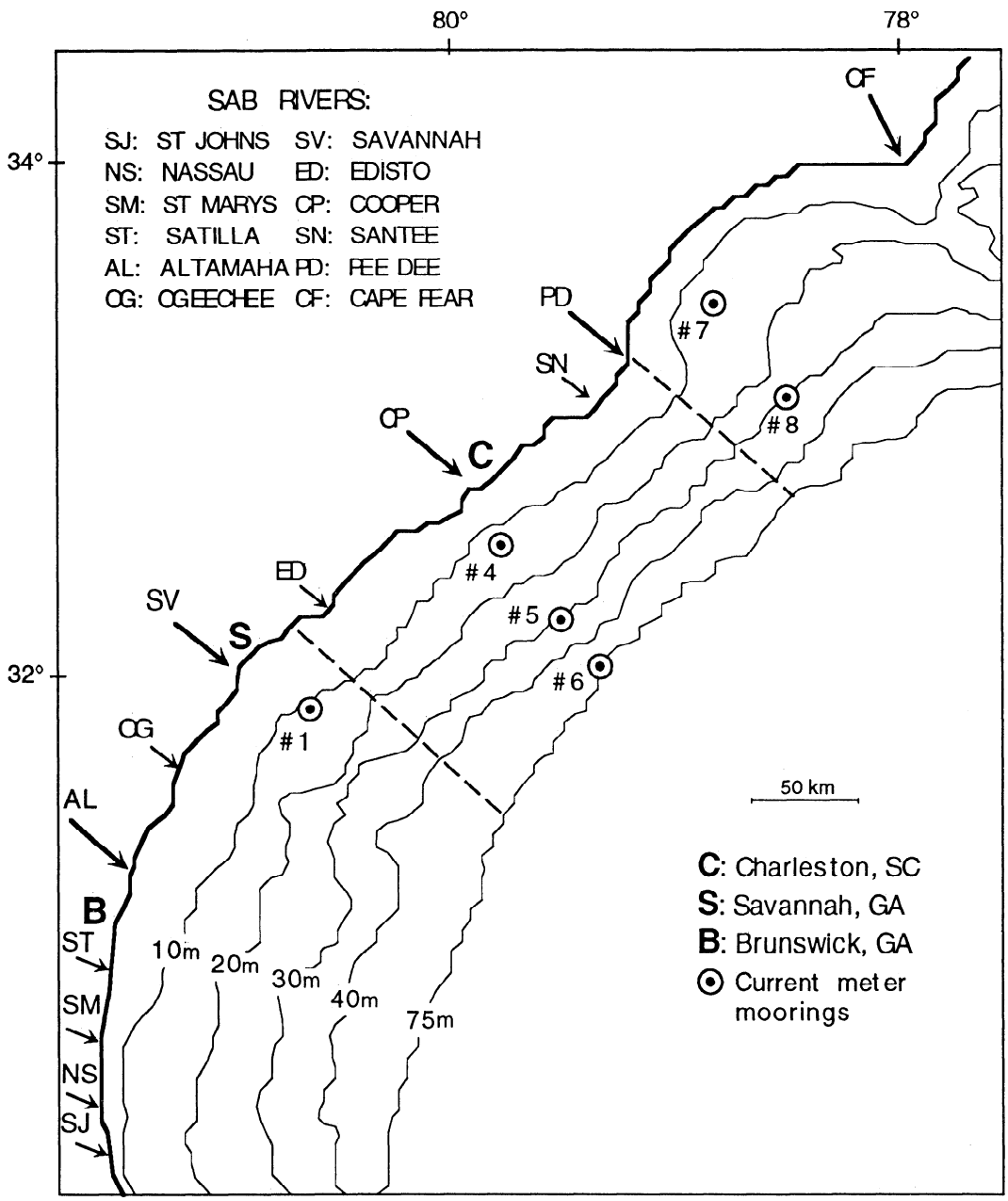

Figure 3. Detail of South Atlantic Bight (SAB) model area (model subdomain marked in Figure 1), which includes the 12 major SAB rivers (large rivers marked by long, thick arrows). The dashed lines define the area of the pre-Spring Removal Experiment (pre-SPREX) hydrographic surveys. The current meter mooring locations are marked by circles.

station data to suitably represent the effective wind magnitude and direction over water.

3.2. Model Initialization Run

A wintertime salinity distribution was simulated based on data for the winter of 1984. The initialization run started from rest, constant temperature T=18°C, and constant salinity S=35 ppt. The model was then integrated for 60 days, forced by river discharge (mean January runoff for each river) and tides. The length of the integration was determined by the time it took the model to form a low-salinity band along the inner shelf, forced by the moderate January discharge. As is shown in Plate 1a, the 34.8 and 34.5 parts per thousand (ppt) isohalines extended along the nearshore shelf domain, connecting the individual plumes of rivers (except the Cape Fear river plume). Results from this and the next section are plotted on the model subdomain presented in Figure 3.

The initialization run was continued for 30 more days, with daily river runoff and additional forcing by wind (6-hourly values), representing February 1984. The freshwater input during February underwent significant reduction from the January mean values, and all rivers exhibited minimum discharge around the middle of the month (Figure 4). The wind stress field contained frequent reversals in direction, which is characteristic of the winter season, due to the

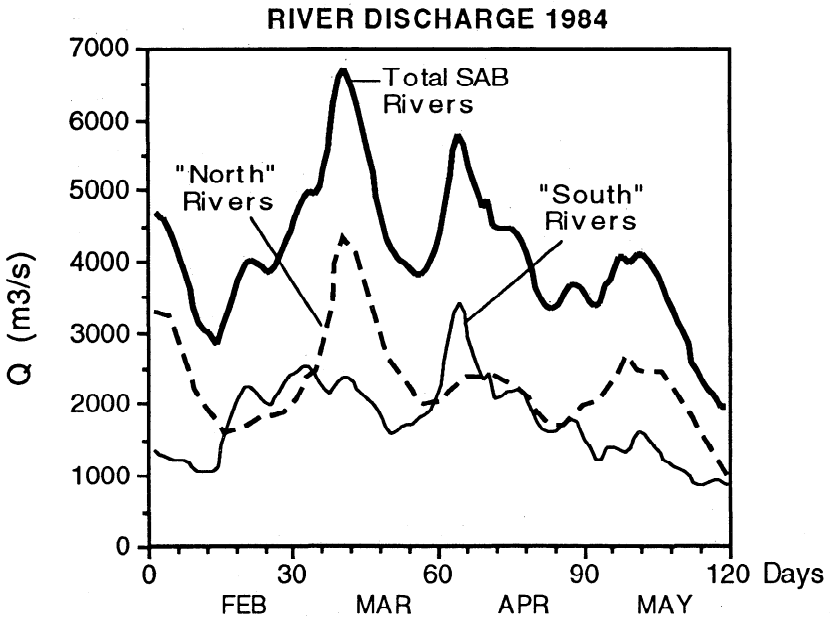

Figure 4. Total river discharge during the spring of 1984; all SAB rivers (thick solid line); "north" (dashed line) for all rivers north of Savannah River, and "south" (thin solid line) for the Savannah River and all rivers to the south (based on data from *Kourafalou* [1993]).

passage of cold fronts and low- pressure systems. The near-surface salinity field at the final day of the initialization run (t=90 days, March 2, 1984) is shown in Plate 1b. At that time, the boundary between low-salinity and ambient shelf waters was close to the 20 m isobath (offshore extent of the inner shelf). A continuous low-salinity band (salinities < 34 ppt) was formed from the Pee Dee River at Cape Romain to the St. John's River off north Florida, while lower-salinity patches (salinities < 30 ppt) were evident in front of the river mouths (see Figure 3 for river locations). The Cape Fear River plume remained distinct from the low-salinity band, although fairly close, as the 34.8 ppt salinity contour indicates. No significant offshore removal of the low-salinity band was detected, as the wind field exhibited frequent downwelling-favorable events, while the most persistent upwelling-favorable wind event coincided with the lowest February runoff.

3.3. Realistic Numerical Simulation

We simulate the response of the low-salinity band to the changes in freshwater discharge and wind stress conditions during the first 2 months of spring 1984 (March and April). The model was initialized with the SAB velocity and density fields of section 3.2 that represented "winter" (end of February) conditions. The forcing included daily values of river discharge, 6-hourly values of wind stress, and semidiurnal tides.

The 2-month period of the realistic simulation (March 3, 1984, to May 2, 1984) was divided in twelve 5-day periods in order to facilitate the discussion of results. We examined the model results on a day-to-day basis, but we decided that, rather than presenting characteristic "snapshots" of model output, it was more practical to give an overview of the calculated fields by summing them up in equal, though arbitrary, time periods. The model-computed salinity and velocity fields were averaged, first, semidiurnally in order to filter out the effect of M_2 tides, then, over each of the 5-day periods. Two more periods were analyzed that covered the duration of the pre-SPREX hydrographic surveys. The complete series of modeled salinity fields has been illustrated by *Kourafalou* [1993]. We have selected the following five representative examples to present herein: March 13-17 (period A), March 18-22 (period B), April 7-11 (period C), and the two pre-SPREX hydrographic periods D (April 14-18) and E (April 21-24). Figure 5 shows the following features of the time-dependent river discharge and wind field model forcings. The beginning of the realistic simulation, where the first peak in freshwater input occurred, was characterized by weak and rapidly varying winds. Typical springtime conditions appeared during the end of March and over most of April, when the winds became stronger and mostly upwelling-favorable. An exception was the significant downwelling-favorable wind event during April period C, which took place soon after the second peak in river discharge.

Plate 2 presents the model-computed, near-surface current and salinity fields during March period A. The high river discharge that preceded this period was still present and created the large amounts of low-salinity water that are found near the major rivers. The atmospheric conditions, however, were not favorable for offshore removal of this water due to the small magnitude and rapid direction reversals of the wind stress vector. The low-salinity band was thus contained within the inner shelf and the currents were mainly buoyancy-driven, exhibiting a strong offshore component near the river mouths and a southward (alongshore) flow, which was strongest in the south part of the domain, where several small rivers combine their plumes with the major Altamaha River. The absence of wind-driven currents is evident in the deeper parts of the shelf and away from the rivers in the inner shelf.

Plate 3 shows the surface velocity and salinity averaged

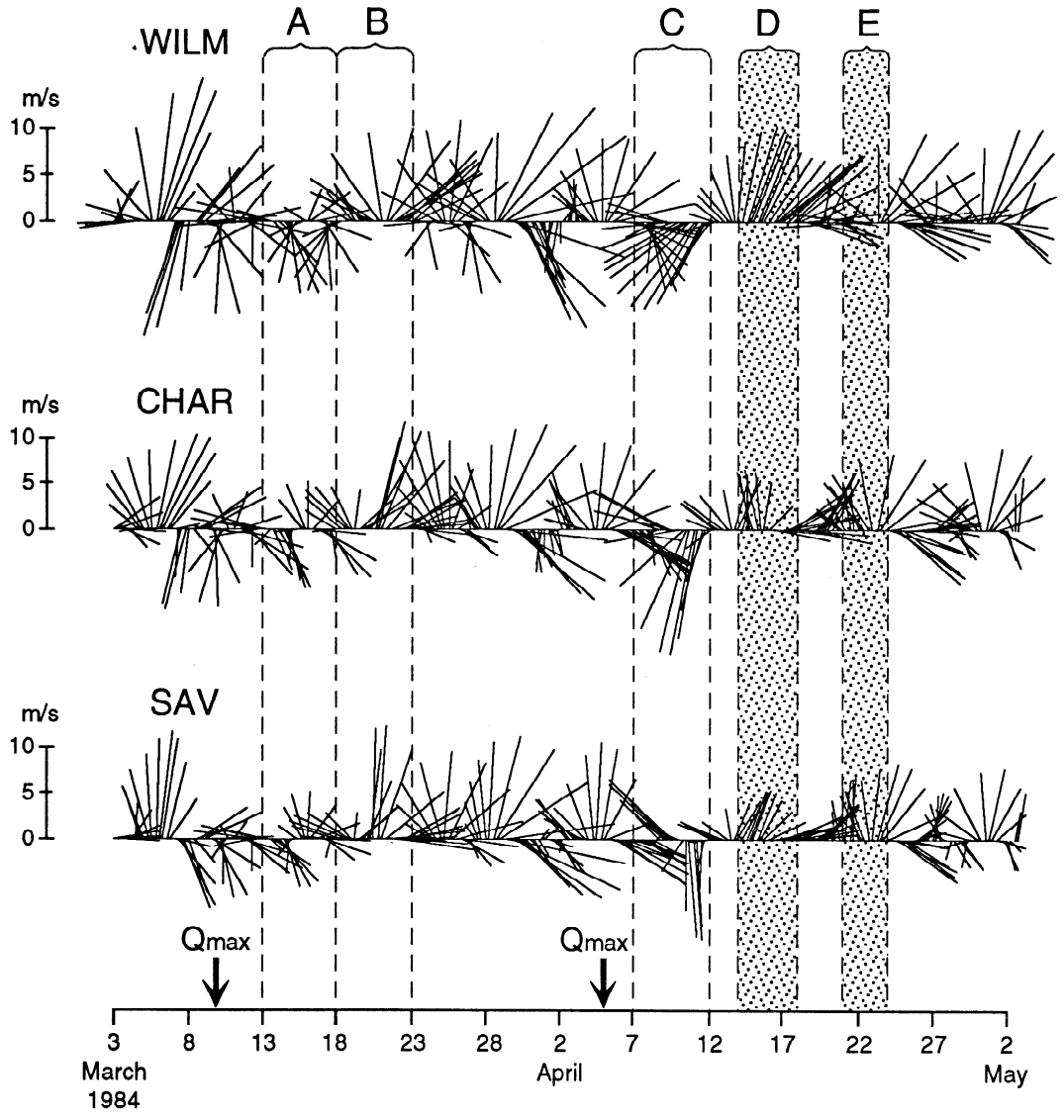

Figure 5. Examples of the calculated wind forcing, derived from coastal stations and applied on the adjacent shelf areas, near (top) Wilmington, North Carolina, (middle) Charleston, South Carolina, and (bottom) Savannah, Georgia. The two maxima in total river discharge Q are marked. The dashed lines define five simulation segments discussed in text. Periods D and E are stippled, and they correspond to the first and second part of the pre-SPREX hydrographic survey, respectively.

over March period B. The freshwater supply from the rivers is currently diminished, but there is still a considerable amount of low-salinity water near the coast. This is due to high discharge during the previous 15 days, indicating that the "history" of the river input is important. The wind field marks the first significant upwelling-favorable event during the 2-month simulation. Accordingly, this period contains the first noticeable northward and offshore removal of the low-salinity band.

Plate 4 (April period C) includes the strongest downwelling-favorable wind event during the realistic simulation. This period follows the second peak in SAB river discharge. Consequently, a large amount of low-salinity water was present. The buoyancy-driven southward flow combined with the wind-driven southward flow to create strong onshore transport. The significance of this event was that large amounts of low-salinity water "piled up" against the coast. As soon as the wind shifted to upwelling-favorable (see below), the coastally trapped waters were removed and a dramatic offshore displacement of the entire low-salinity band took place.

Plates 5 and 6 are composites of model-computed surface velocity and salinity fields during the two pre-SPREX hydrographic survey periods D and E. Both surveys took place during the most persistent upwelling-favorable wind event during the spring of 1984. The average values of both river discharge and wind were greater during period D, while the average wind direction was positive and alongshore during both D and E. Although the actual river discharge gradually diminished, there was a large volume of available low-salinity nearshore water due to the preceding events: high discharge and several days of onshore surface transport. This was particularly evident near the mouths of the major rivers, where the lowest-salinity water was

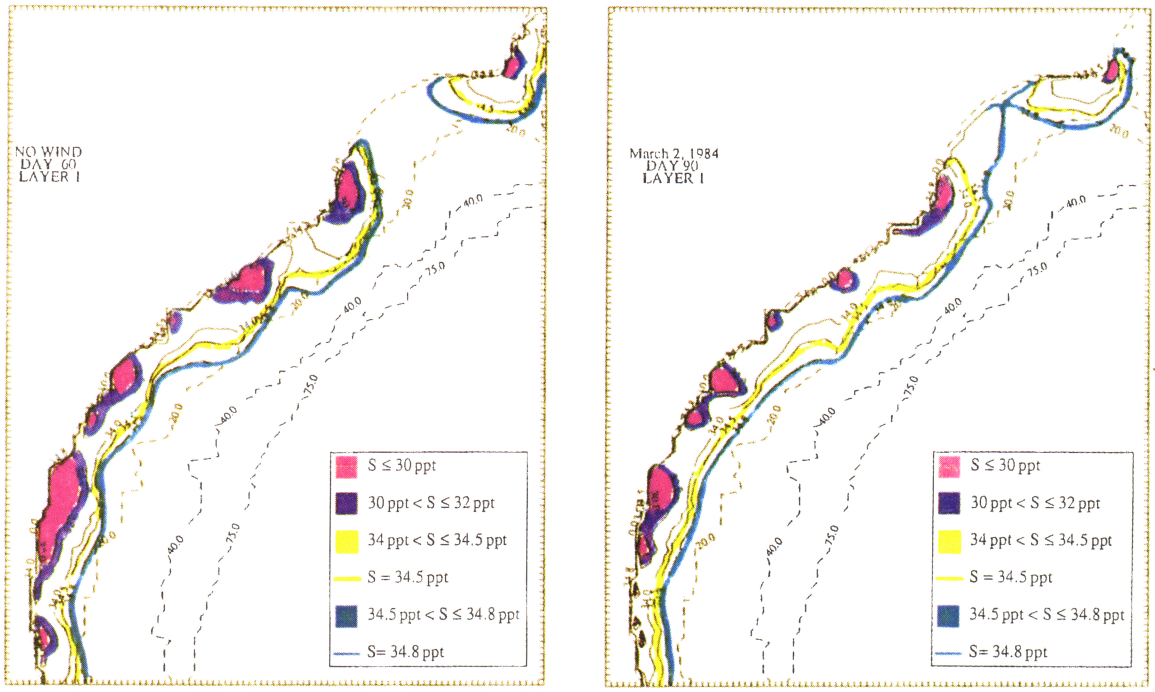

Plate 1. Model-computed, near-surface salinity contours during initialization run, with forcing of (a) constant river discharge (January mean), tides, and no wind and (b) river discharge (daily mean), tides, and wind (6-hourly data). Dashed lines are isobaths.

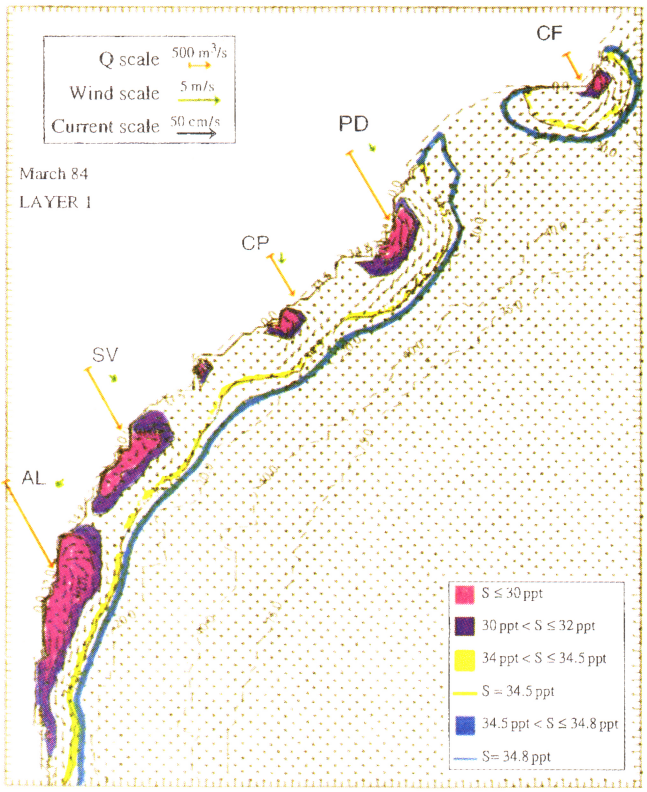

Plate 2. Model-computed, near-surface velocity and salinity fields, averaged over March period A (March 13-17). The red arrows mark the 5-day-averaged river discharge, and the green arrows mark the 5-day-averaged wind vector in the vicinity of rivers (winds are unrotated, that is, "upward" vector points toward north). Dashed lines are isobaths.

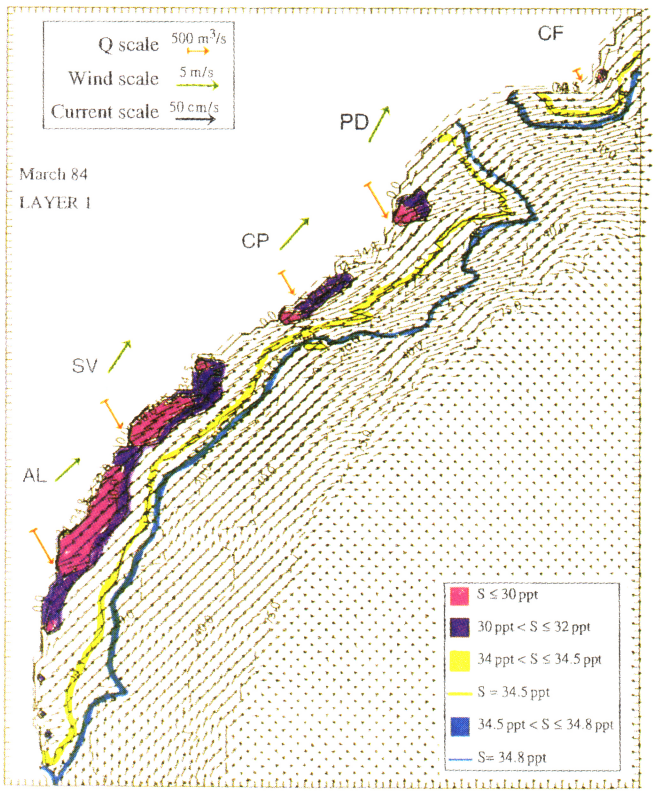

Plate 3. Same as in Plate 2, but for March period B (March 18-22).

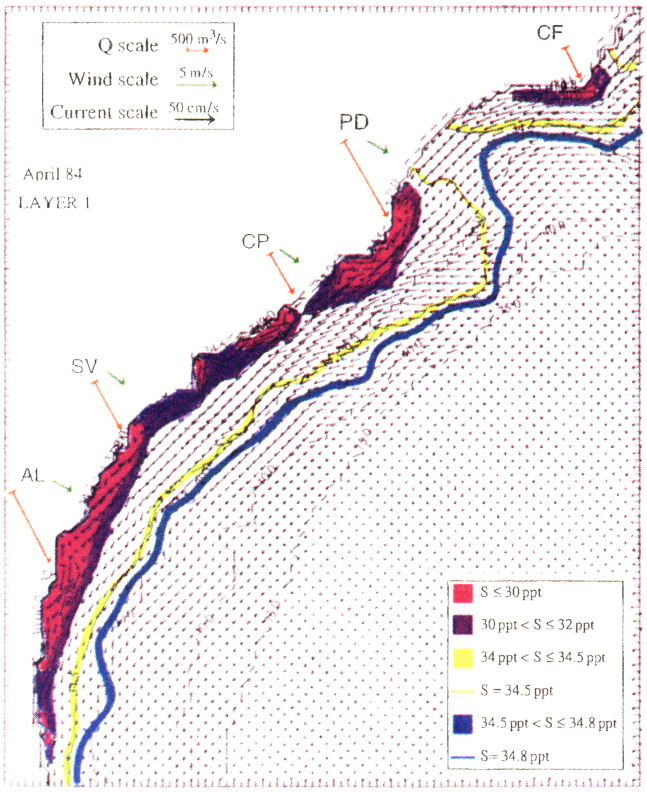

Plate 4. Same as in Plate 2, but for April period C (April 7-11).

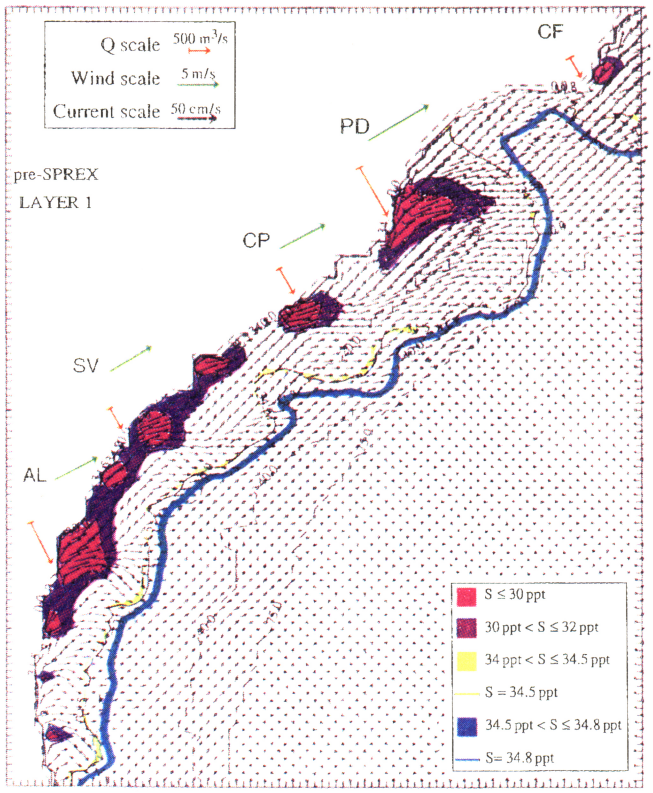

Plate 5. Same as in Plate 2, but for pre-SPREX period D (April 14-18).

found. A flow pattern of jetlike offshore "streamers" was observed in the vicinity of rivers. It was created by the decoupling of surface and bottom layers within the nearshore pools of highly stratified coastal waters. This led to increased wind- imported momentum to the upper layer, which, combined with the buoyancy-driven flow, created regions of intensified offshore flow. Satellite imagery has shown that this "tonguelike" distribution of coastal shelf waters happens during spring as a transient rather than persistent pattern. This is supported by our simulation, which showed that the streamers formed only during the high discharge and persistently upwelling-favorable wind conditions that characterize the spring season. They were mainly near-surface features, as they generally occupied the upper third or quarter of the water column beyond the nearshore region. They were also short-lived, as they were substantially modified a few days later (compare Plates 5 and 6). However, they contributed to the significant offshore removal of riverine waters that is marked by the displacement of the low-salinity band as far offshore as the outer shelf and shelfbreak during this period.

Plate 6 shows "lenses" of water with salinity less than the ambient advected across the shelf. This phenomenon occurred throughout the simulation, but in this incident the lenses were larger in volume and persistent enough to be detected. In both periods D and E the offshore surface transport was most pronounced in the northern part of the model subdomain, off Cape Romain. This is the combined result of river location and the local variability in wind and buoyancy forcings. Cape Romain is the discharge site of

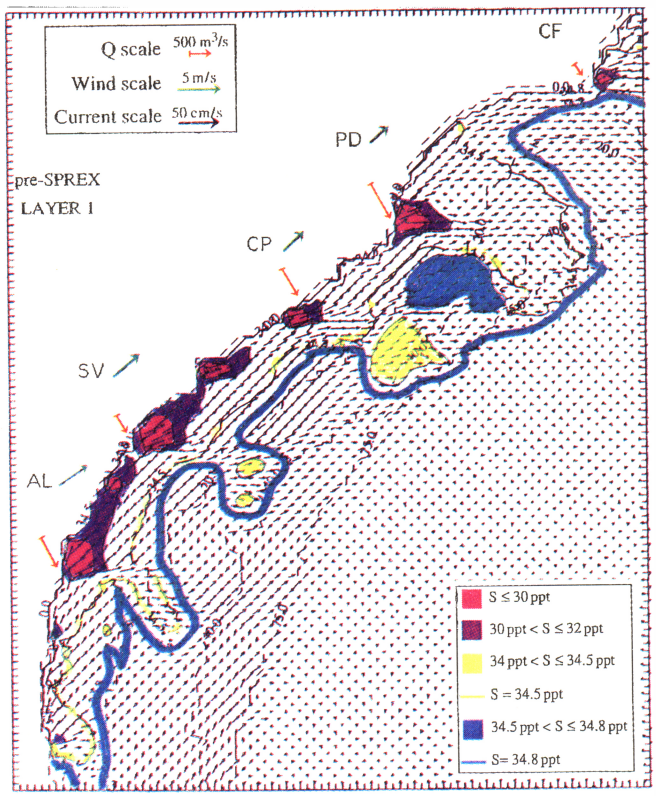

Plate 6. Same as in Plate 2, but for pre-SPREX period E (April 21-24).

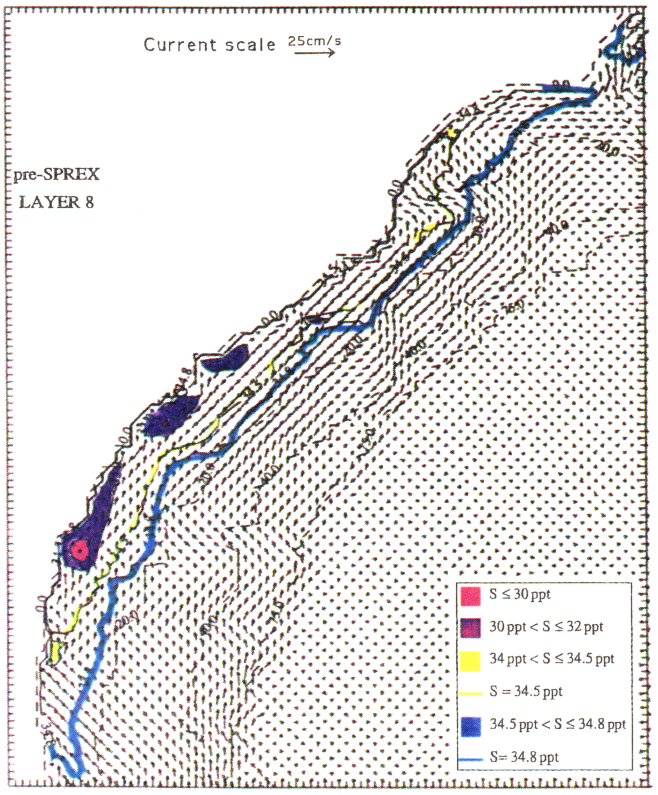

Figure 7. Salinity contours based on the pre-SPREX hydrographic data. (top) Near-surface horizontal view for period (left) D and (right) E. (bottom) Vertical view at a shelf cross section off Charleston, South Carolina, for 1 day during survey period E.

the major river Pee Dee, which forms the "head" of the SAB coastal low-salinity band (the Cape Fear River plume is only occasionally part of the band, as shown in Plates 2-6). As can be seen in Plate 5, both local discharge (river Pee Dee) and local (positive alongshore) wind stress were strongest in the vicinity of Cape Romain during period D. The consequent strong offshore transport was intensified by the contribution of the rivers south of Pee Dee. According to the process studies of *Kourafalou et al.* [this issue], the offshore transport during upwelling-favorable wind stress is pronounced at the "head" of a line source of freshwater input. The shoaling isobaths north of Cape Romain, i.e. in the vicinity of Cape Fear, also supported the offshore veering of the wind-driven transport.

An example of near-bottom calculated velocity and salinity fields is given in Plate 7 for period E. The currents are weaker than near-surface and the predominant flow is in the direction of the wind. Within the strongly stratified areas, however, onshore flow is observed, which compensates for the offshore surface flow. The tendency for near-bottom opposite flow in the stratified shelf was evident during the entire calculation, and it was responsible for the confinement of the lower layers of the low-salinity band within the inner shelf. Plate 7 shows that the lowest-salinity water during the second hydrographic period was found in the south part of the model domain. This also seemed to hold during most of the simulation, and we attribute it to two reasons. First, this area receives the combined input of several neighboring rivers, including the major Altamaha and Savannah Rivers. Secondly, since the M_2 tides are strongest in this part of the shelf (Figure 2), the freshening of nearshore waters is often carried by the tides over the entire water column. The most favorable conditions for freshening of the nearshore bottom layers throughout the domain were obviously during downwelling-favorable winds.

Vertical cross sections of model-computed salinity during the second hydrographic survey period E are presented in Figure 6. Figure 6a is taken through the largest offshore displacement of isohalines (streamer) off the Pee Dee River shown in Plate 6. Vertical stratification is present in the upper third of the water column over the entire domain. The 10 m isobath roughly corresponds to the seaward edge of the nearshore low-salinity band, where stratification is strongest both horizontally and vertically. Figures 6b - 6d were taken perpendicular to the coast. The vertical distribution of salinity in Figure 6b corresponds to the Charleston cross section and agrees qualitatively with a similar section during the pre-SPREX II shipboard measurements, shown in Figure 7. The salinity distribution in Figure 6c, which is taken north of Savannah and away from rivers, exhibits no stratification in the vertical and much less low-salinity water near the coast. Finally, Figure 6d, across the Savannah River, displays a nearshore low-salinity area, horizontal stratification in the inner shelf, and a midshelf vertically stratified lens that is part of the Savannah streamer (Plate 6). The vertical salinity patterns indicate that the areas of strong surface offshore displacement of the nearshore low-salinity band are accompanied by the strongest vertical stratification on the shelf and occur seaward of the major river discharges.

The model-computed salinity fields on the full SAB grid domain (illustrated by *Kourafalou* [1993]) can be summarized as follows. The alongshore extent of the low-salinity band generally covered the coastal area between the north part of South Carolina and the north part of Florida (approximate length, 600 km). The maximum southward extent was only about 40 km south of the St. John's River (around St. Augustine, Florida), and it occurred during the strong downwelling-favorable event presented above (April period C). The maximum northward extent was observed whenever the Cape Fear River plume joined the low-salinity band, and it reached as far north as Cape Lookout, North Carolina. However, it must be noted that during the entire simulation the Cape Fear plume was either distinctly independent or it occasionally merged at the 34.8 ppt isohaline with the rest of the rivers. Therefore it can be excluded from the main area of the low-salinity band, which thus extended as far northward as Long Bay between Cape Romain and Cape Fear.

The modeled current fields on the full SAB domain (not shown) were influenced by wind stress, stratification and bottom topography. They generally followed the patterns that were discussed during the process studies on the interaction of buoyancy and wind stress forcings in Part 1. Examination of daily computed flow fields suggested that the variability on the shelf during the spring season was greatly influenced by the amount and the location of low-salinity waters that resulted from river runoff. Buoyancy-induced stratification caused the decoupling between "top" and "bottom" Ekman layers, thus intensifying the

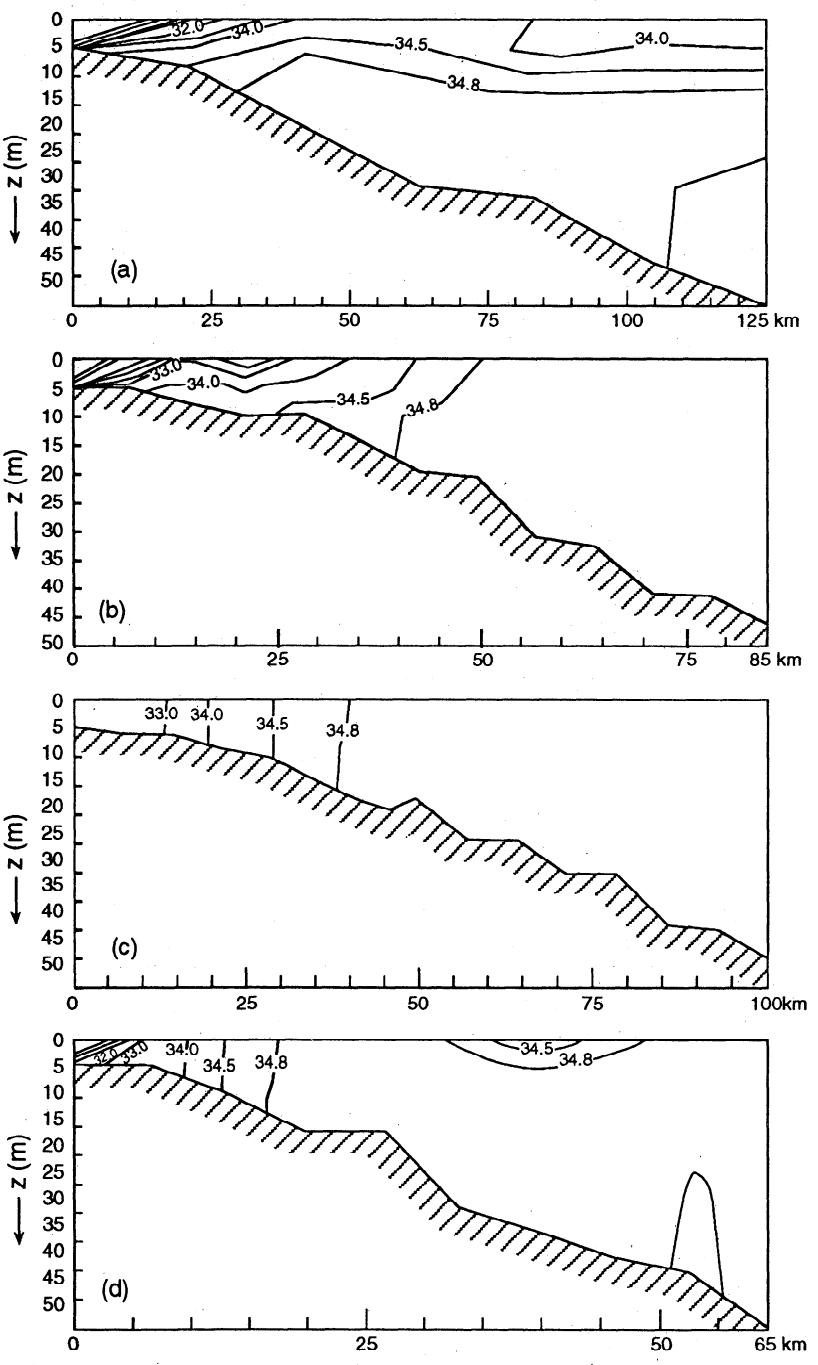

Figure 6. Vertical sections (depth versus offshore distance) of model-computed salinity during the pre-SPREX period E (April 21-24), (a) across the "streamer", (b) across the shelf off Charleston, South Carolina, (c) across the shelf away from rivers, and (d) across the shelf off Savannah, Georgia.

acceleration of the surface flow by wind. When the freshwater input was strong enough to withstand opposing wind stress, however, a southward buoyancy-driven current was present within the influence of the river plumes, while other shelf areas could be entirely wind-driven in the opposite direction. This was mostly evident in the shelf area south of Savannah, which receives not only the strong local runoff, but also low-salinity waters advected from the rivers farther north. When the buoyancy input was weak, areas of opposing surface currents were occasionally detected during periods of flow adjustment to wind reversals, where nearshore waters responded to the "new" wind direction faster than those farther offshore.

4. Discussion of Results

4.1. Comparison to pre-SPREX Data

The salinity fields that were derived from ship measurements during the two pre-SPREX surveys are presented in Figure 7 [from *Paffenhoffer et al.*, 1994]. The area that was sampled during the experiment was at the "north" part of the shelf in the vicinity of Cape Romain (marked by the dashed lines in Figure 3), where the most pronounced offshore movement of low-salinity water was expected. The shipboard measurements show that the boundary of the low-salinity band extended to the outer shelf during the first survey and even farther during the

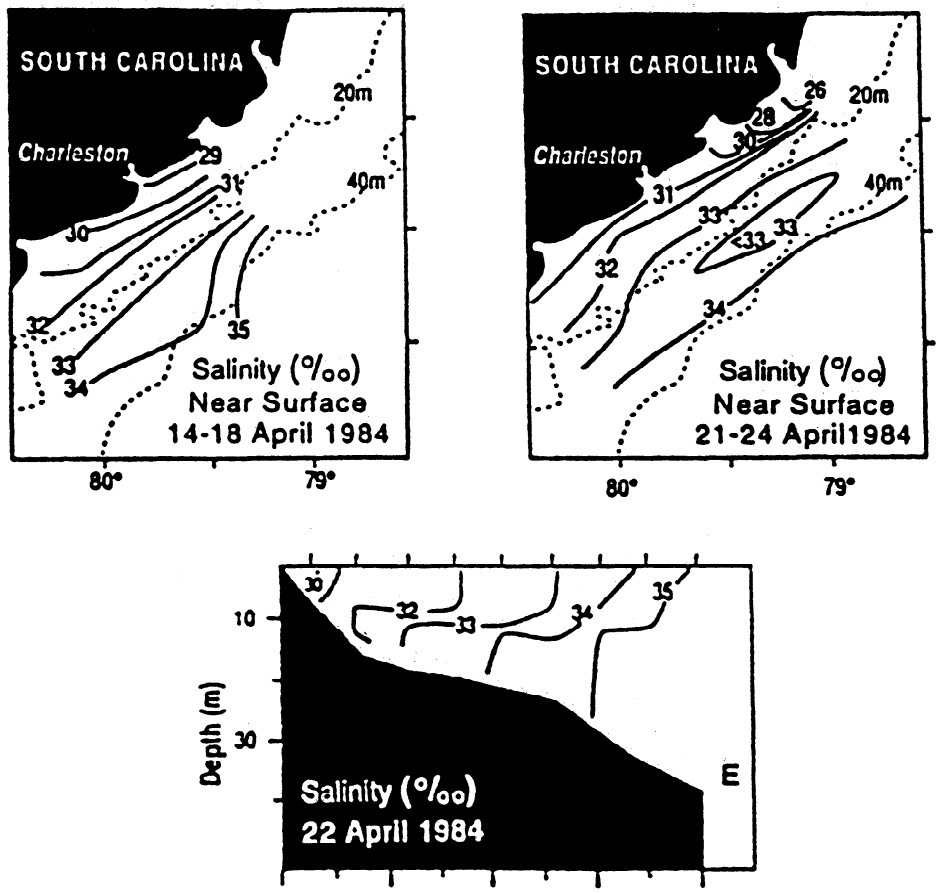

Figure 7. Salinity contours based on the pre-SPREX hydrographic data. (top) Near-surface horizontal view for period (left) D and (right) E. (bottom) Vertical view at a shelf cross section off Charleston, South Carolina, for 1 day during survey period E.

second survey. This is in agreement with the model-computed distribution of salinity (Plates 5 and 6). The lowest-salinity water (≤32 ppt) was found slightly farther offshore in the hydrographic data (close to the 15-m isobath) as compared with the model results, where it reached the 10-m isobath. Qualitatively, the evolution of the low-salinity band is quite similar in model and data. An offshore lens of coastal water (<33 ppt) is observed in the second survey off Charleston, similar to the numerical simulation, where lenses of nearshore water were found offshore. Figure 7 (bottom) gives a snapshot of vertical distribution of salinity, using data averaged over one of the days during the second pre-SPREX survey period E. There is qualitative agreement with the model vertical salinity contours in Figure 6b, which were plotted on the same cross section, through Charleston. However, the survey data do not offer a conclusive validation of model results, due to the strong time and space variability of the salinity field, the limited amount of hydrographic data, and the small area that the surveys covered.

A more rigorous assessment of the computed fields can be achieved by comparing time series of model- and data-derived currents. Low-pass-filtered, moored current meter data were available for the 2 months of the realistic model simulation. The corresponding model-computed currents were derived at comparable grid locations and for the same depths as the instruments. The current meter locations are shown on the model grid in Figure 3. Two near-surface current meters are available at moorings 7 and 8. As the mooring locations are fixed, the measured flows are intermittently inside or outside the "core" of the neighboring river plumes. Although a more detailed mapping of the river-induced low-salinity band would be desirable, we believe that the model-to-data comparison based on the available current meter data is valuable.

Daily averaged values were used for both model and data velocities, so that M_2 tidal variability was filtered out. All records were rotated according to the local isobath orientation in order to highlight cross-shore and alongshore motions. Detailed time series at each mooring position are given by *Kourafalou* [1993]. The following three representative examples are presented herein: near-surface currents at mooring 7, middepth currents at mooring 5, and near-bottom currents at mooring 4. The modeled and measured time series for the cross-shore u and along-shelf v velocity components are given in Figures 8 and 9, respectively. The agreement is remarkable in both the inner shelf (moorings 4 and 7) and the midshelf (mooring 5) locations. The model reproduced the along-shelf flow very well, especially in the phase of the response to wind events, while the magnitude was occasionally smaller. The u component flow comparison is also quite satisfactory, considering that cross-shore flows are typically weak and sensitive to the locally considered coordinate system, as

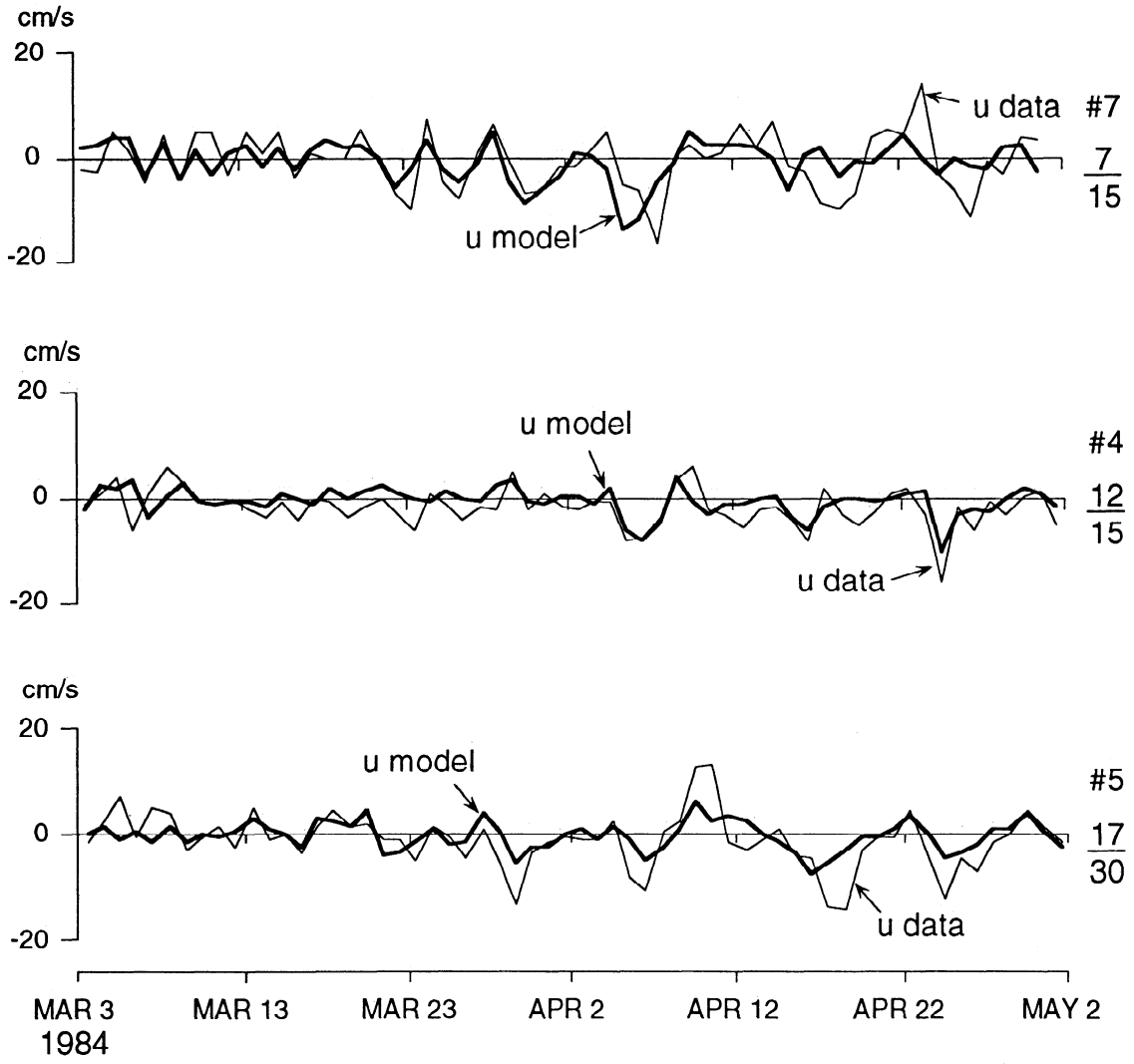

Figure 8. Comparison between model (thick lines) and data (thin lines) cross-shore u velocity time series at the location of moorings (top) 7, (middle) 4, and (bottom) 5. The ratio of measurement depth to water depth is given at the side of each time series.

slight changes in rotation can cause them to be either negative or positive (onshore or offshore).

For further comparison of model and observed currents, a time domain empirical orthogonal function (EOF) analysis was performed with the computed and measured current records from all mooring locations (18 time series all together). The results are presented in Figure 10 for the first mode EOF of the u and v components. This mode accounted for 64% and 91% of the total variance of the low-pass-filtered u and v records, respectively. The alongshore component of the average wind over the mooring area is also shown in Figure 10 and it suggests that the currents were strongly wind-driven. Variance-conserving spectra of the first mode time EOF from the model and observations are illustrated, together with their coherence and phase spectra, in Figure 11. Both model and observed EOFs show well-resolved spectral peaks at periods centered at 3- and 8-day periods (similar to the alongshore wind stress spectrum), with high coherence and near-zero phase. This agreement strongly supports the validity of model results.

4.2. Momentum Balance

We computed the daily and vertically averaged momentum terms from data and model at the mooring locations. The most representative momentum balance (near "steady" state) occurred after flow adjustment to wind shifts, i.e., after a few days of persistent wind forcing [*Kourafalou*, 1993]. In Plate 8 we present a characteristic example at the end of an upwelling-favorable wind event (March 22, 1984, see Figure 5) and for the location of the inner shelf current meter across Charleston (mooring 4; see Figure 3). The wind record from Savannah Light Tower was used for the data-derived wind stress, and coastal sea level measurements from Charleston and Savannah, along with bottom pressure measurements from the outer shelf mooring 6, were used for the calculation of the pressure gradient term. Measured currents from moorings 1, 7, and 8 provided the needed spatial velocity gradients. The derivation of the model momentum terms is the same as that of *Miller* [1992]. The magnitude of each term is shown as a vertical bar in Plate 8, while the sum of all

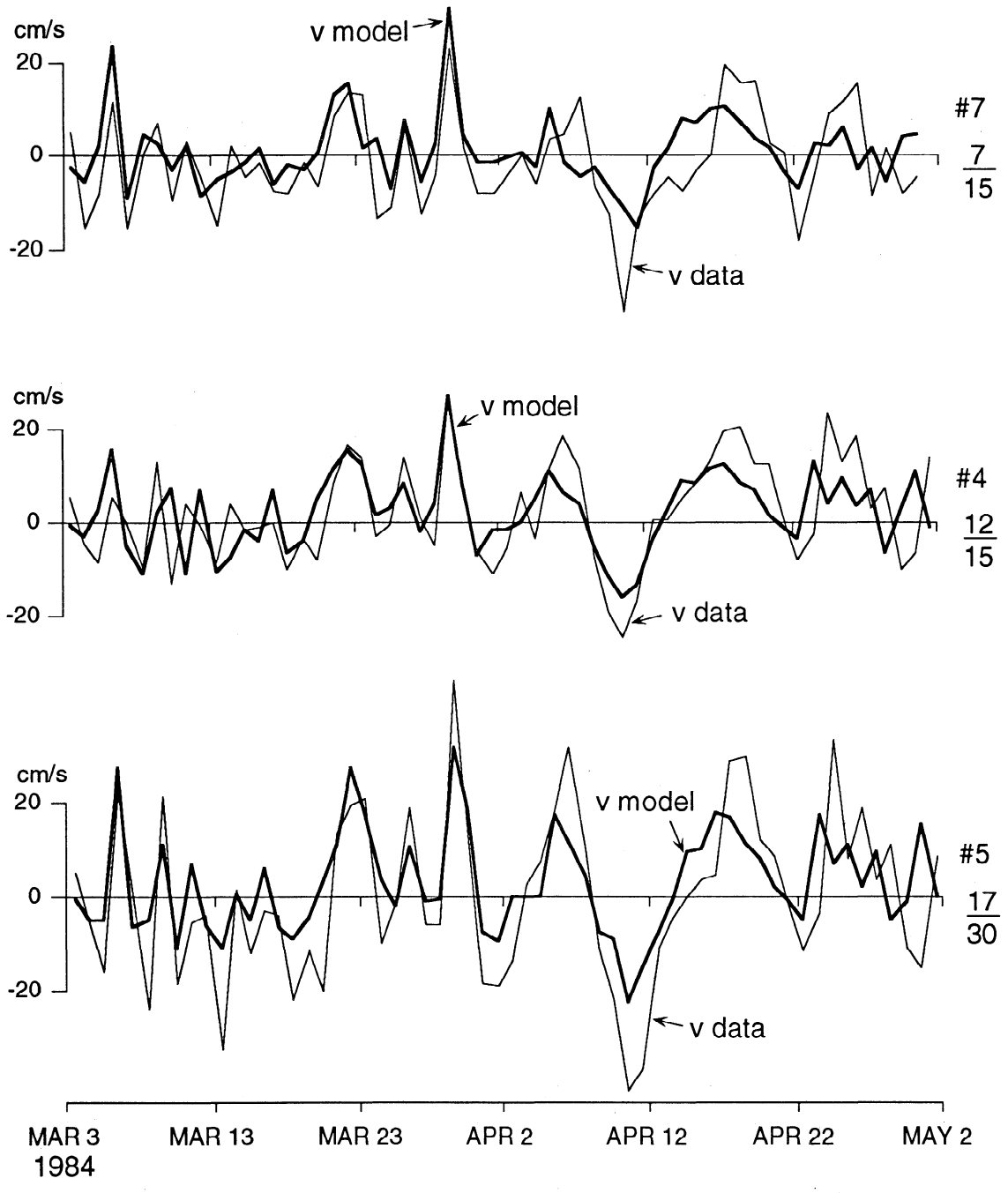

Figure 9. Same as Figure 8, but for the alongshore v velocity component.

terms is also shown as an indicator of residual ("unbalanced") acceleration.

The x momentum estimated terms suggest a "quasi-geostrophic" balance between cross-shore pressure gradient, Coriolis, and cross-shore wind stress. In the model-based calculation the "sum" is very small, while the larger value of sum in the data derivation is due to the lack of vertical resolution in the current measurements (resulting in error in the Coriolis term) and the crude representation of the pressure gradient term. The moored current meters provided measurements mostly in the lower depths, so any data-based, vertically averaged flow was generally smaller in the alongshore direction, while smaller and sometimes of opposite sign in the cross-shore direction. The model-derived averages and gradients were, on the other hand, well resolved both vertically and horizontally. The data momentum balance did not include the vertical advection, horizontal friction, and baroclinic pressure gradient terms, which are shown in the model balance and are generally small. The contribution of the bottom stress term is also relatively small in model and data alike.

The model derived y momentum terms expressed a balance between Coriolis acceleration, alongshore pressure gradient, local acceleration, and alongshore wind stress opposed by almost equal bottom stress. The data estimate, however, had a sum value that was comparable to the large wind and bottom stress terms, apparently due to errors in estimating the Coriolis and pressure gradient terms as explained above.

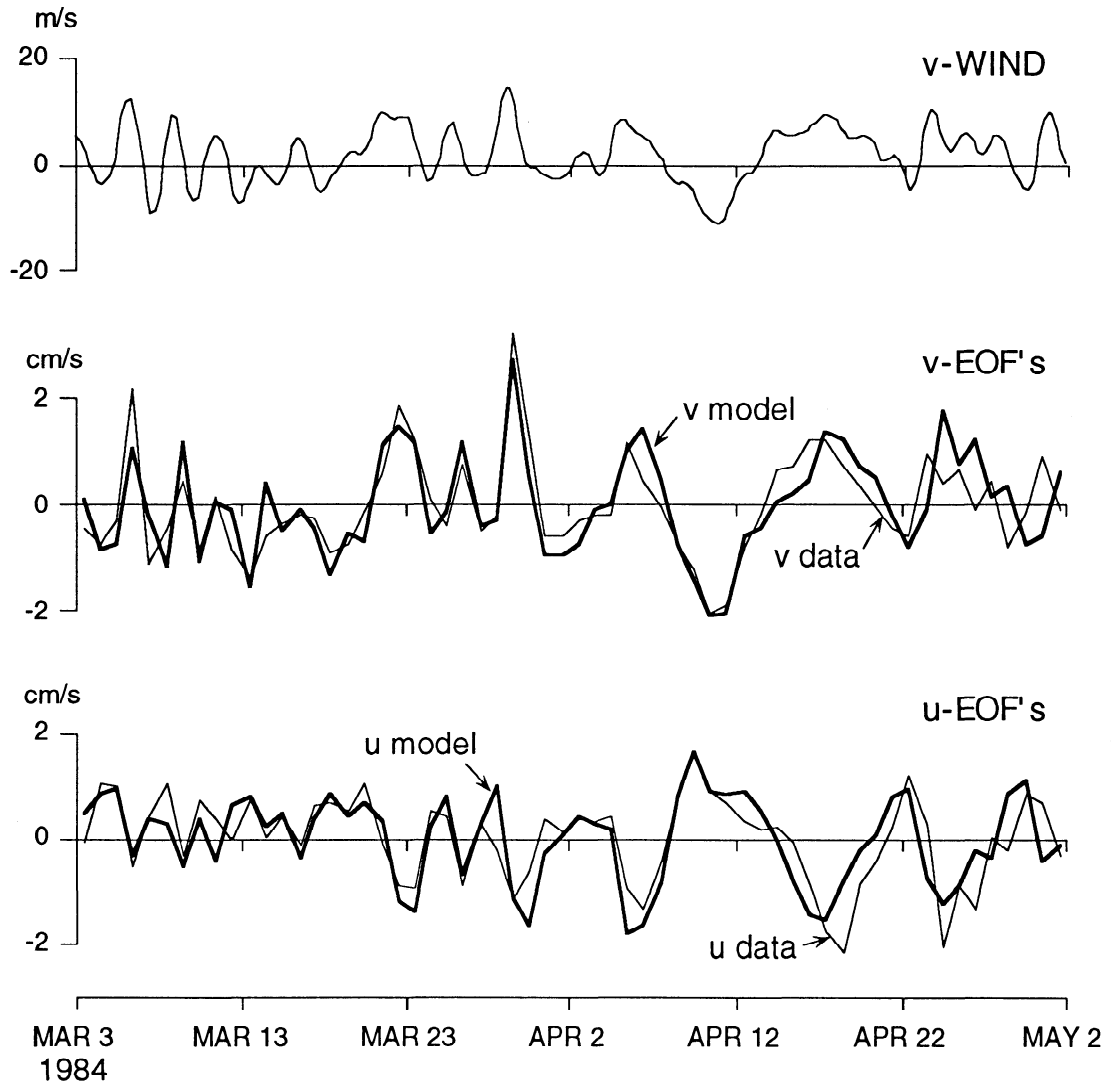

Figure 10. Empirical orthogonal function (EOF) time series comparison between model (thick lines) and data (thin lines) for (middle) *v* components and (bottom) *u* components. (top) The *v* component of the wind averaged over the mooring area.

4.3. Model Performance Evaluation

The model computed realistic flow patterns for the variety of dynamical processes that were combined herein. The model exhibited the ability to accommodate various scales, both in space (shallow coastal and deeper shelf and ocean regions, depth range 2-1000 m) and in time (small-scale turbulence to tidal and wind-driven motions). The model-to-data comparison of currents at various shelf locations and different depths showed very good agreement, not only in the prevailing alongshore flow, but also in the cross-shore flow and for both inner shelf and midshelf regions. First-order statistics were computed for the alongshore and cross-shore velocity component time series (Table 2a) and the first-mode EOF time series from both model and data (Table 2b). Mean flows agreed within 2 cm s^{-1} and were in the same direction. The mean was removed in the EOF analysis, so it is shown as zero. Standard deviations of the EOF time series from data and model were almost identical, with differences of only 2.0%. Standard deviations and rms error of model time series were within 2 cm s^{-1} of the these statistics computed from individual current meter records for both alongshore and cross-shore components. The model comparisons with individual current meter records are quite satisfactory, considering they are point comparisons over a 2-month period in 3-D ocean/model space where the vertically and horizontally stratified flow is constantly changing.

A detailed comparison of salinity fields was not possible due to the limited amount of hydrographic data, although a qualitative agreement of model and data was evident. Further verification of the model-simulated salinity fields was sought via coastal zone color scanner (CZCS) pictures of near-surface chlorophyll concentrations during spring 1984. The chlorophyll has been successfully utilized as a tracer of the nearshore low-salinity band [*McClain et al.*, 1988]. We present an example in Plate 9, where a visual comparison of the coastal concentrations for early March and early April 1984 is feasible. The larger offshore displacement of the low-salinity band in April provides further qualitative verification of the numerical simulation results, where significant widening of the coastal band started toward the end of March and continued through April.

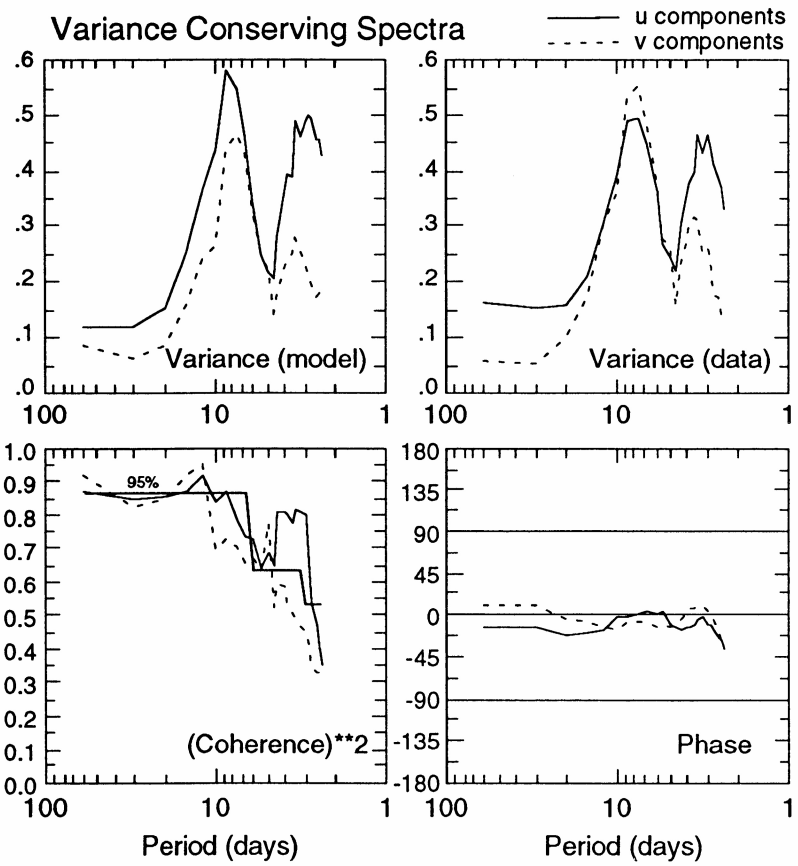

Figure 11. Variance-conserving spectra (first mode EOF) for the model and data *u* components (solid lines) and *v* components (dashed lines).

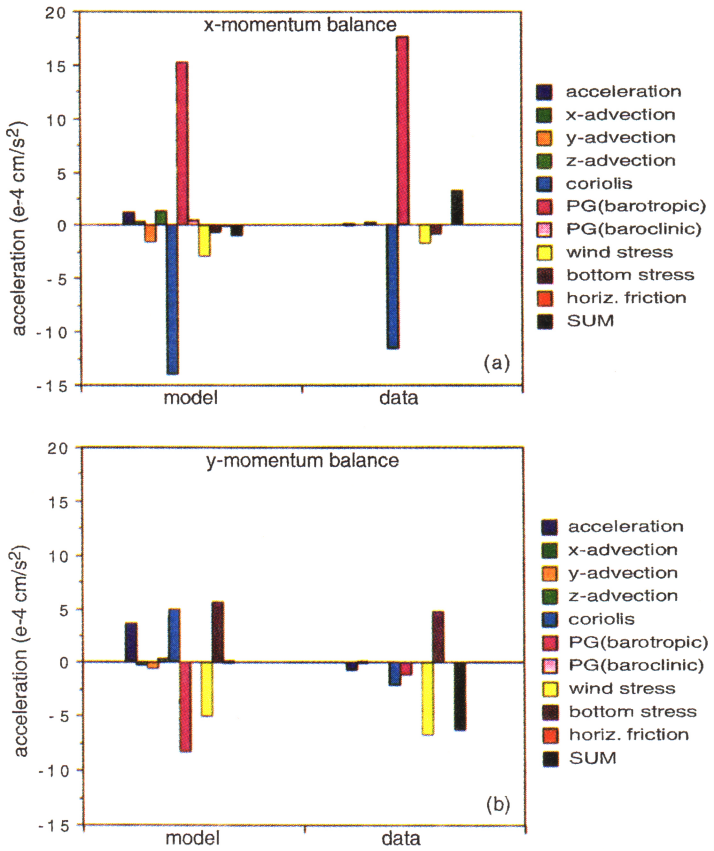

Plate 8. Momentum balance comparison between model (left bars) and data (right bars) and for the (top) across-shore and (bottom) alongshore directions. All momentum terms were calculated in reference to the location of mooring 4 and for the daily averaged values on March 22, 1984.

Table 2a. Comparison of First Order Statistics of Observed and Modeled Currents in the Inner Shelf

				Mean, cm s^{-1}		Std. dev., cm s^{-1}		rms, cm s^{-1}	
Mooring	D, m	d, m	Current	Data	Model	Data	Model	Data	Model
1	15	12	u	-4.6	-1.6	3.8	2.8	6.0	3.3
1	15	12	v	3.4	2.2	7.0	5.0	7.7	5.5
4	15	12	u	-1.7	-0.6	3.6	2.6	4.0	2.7
4	15	12	v	3.2	2.4	10.2	8.3	10.7	8.7
7	15	7	u	-1.8	-0.7	5.5	3.8	5.8	3.9
7	15	7	v	-0.1	1.2	9.2	7.8	9.2	7.9
7	15	12	u	-3.3	-2.5	6.4	5.8	7.3	6.3
7	15	12	v	-2.3	0.0	5.9	4.6	6.3	4.6

D is water column depth, d is instrument depth, Std. dev. is standard deviation, rms is root mean square, u is cross-shore velocity, and v is alongshore velocity.

Table 2b. Comparison of First-Mode EOF Time Series From all Current Meter Locations

	Mean, cm s^{-1}		Std. dev., cm s^{-1}		rms, cm s^{-1}	
Current	Data	Model	Data	Model	Data	Model
u	0.0	0.0	0.8	0.8	0.8	0.8
v	0.0	0.0	1.0	0.8	1.0	0.9

EOF is empirical orthogonal function, Std. dev. is standard deviation, rms is root mean square, u is cross-shore velocity, and v is alongshore velocity.

As stated in the introductory remarks, a major assumption in the modeled circulation was the absence of Gulf Stream forcing. Although modeling of the outer shelf flow, where the influence of the Gulf Stream is strong and persistent, was not an objective of the present study, an evaluation of the consequences of this assumption on the above estimated mean path of low-salinity removal is valuable. As the momentum balance estimates and the time domain EOF analysis showed, the wind-forced barotropic response of the inner shelf and midshelf dominated the dynamics. A net northeastward mean barotropic flow on the SAB south of Charleston, South Carolina, has also been found to originate from an along-shelf surface slope (of negative sign in the northward direction) that is imposed at the shelf edge from oceanic sources, primarily the Gulf Stream [*Kourafalou et al.*, 1984; *Lee et al.*, 1984, *Lorenzzetti et al.*, 1988]. The inclusion of the Gulf Stream in the model would have therefore supported the present findings of a northeastward removal route during spring. We thus expect that the flow patterns and main conclusions of the realistic simulation would remain valid. We speculate that the presence of Gulf Stream forcing could increase the computed transport flow rates, but mainly in the outer shelf and off-shelf regions. The most evident disadvantage of isolating the shelf dynamics from the deep oceanic influence is the inability to examine the fate of riverine water off the shelf. This would have been an interesting calculation, especially in the region off Charleston, where the presence of a cyclonic eddy (Charleston gyre) could cause rapid removal. This eddy has been related to the interaction of the Gulf Stream with the "Charleston Bump" topographic feature [*Bane*, 1983; *Singer et al.*, 1983], which is present in the model's realistic bathymetry.

5. Transport of River-Borne Materials

The freshwater that is brought to the continental shelf by the rivers is both the medium for a number of land-drained tracers of various lifetimes and a relatively long-lived tracer itself. The path that water of river origin follows through the continental shelf can thus be viewed as an indication of the predominant circulation patterns. In section 1 we defined materials as a general term that includes all conservative and nonconservative trace elements, nutrients, sediments, radionuclides, and pollutants. The pathway that river-borne materials is most likely to follow during the spring season is examined here based on the forcing mechanisms that are the focus of the present study, namely, the river runoff, wind stress, and tides. The purpose of this exercise is to offer an application of the model-computed circulation patterns aimed toward the understanding of the extent of impact that land drainage (which is largely controlled by man-related activities) might have on the coastal ocean.

We employ the velocities that were computed during the 2-month realistic model simulation to estimate the path and the fate (final destination) of river-borne particles on

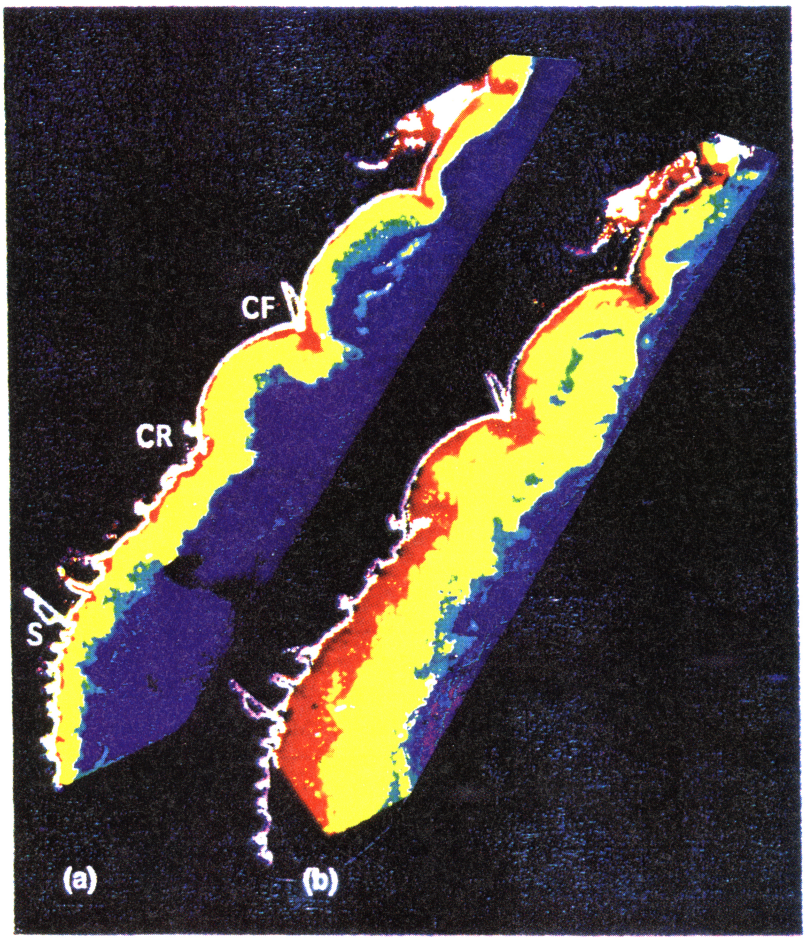

Plate 9. Coastal zone color scanner chlorophyll distributions on the SAB shelf during (a) March 4, 1984, and (b) April 5, 1984 (courtesy of C.R. McClain, NASA Goddard Space Flight Center).

the shelf. As discussed earlier, maximum currents occurred in the surface waters, where the mean flow had a strong offshore component, while the near-bottom currents were weak with a mean onshore direction, which would tend to trap materials deposited in the nearshore bottom sediments. In order to study the maximum possible offshore removal that riverine materials could experience in the SAB during spring, the surface velocity fields were used to compute trajectories of water particles released at the mouth of rivers. For cost effectiveness, the velocities were daily averaged; that is, the M_2 tides were filtered out. The tidal effects were retained through their influence on mixing, which is one of the factors that determines stratification and, consequently, the computed circulation patterns. Sensitivity tests (not shown), where 2-hourly values of velocity (which include tides) were used for the calculation of the trajectories, revealed that the daily mean path of the particles was not altered when the currents were averaged over the semidiurnal tidal period.

During the trajectory simulation the particles were restricted within the upper model layer, and hence the calculated displacements represent surface rather than true Lagrangian trajectories. Although ignoring vertical velocity is an approximation, the surface trajectories do represent a reasonable estimate of maximum offshore distance traveled by a riverine tracer. In order to give a general picture of the offshore removal of coastal water particles, an instantaneous release of two neighboring particles at every SAB river was performed and 2-month trajectories were computed (Figure 12). The displacement tendency was obviously in the northeastward direction, and the preferred area for offshelf removal was approximately between 32° and 34°N as previously hypothesized (section 1). The preferred direction of travel was thus controlled by the mean direction of wind stress and also guided by bathymetry. The particles tended to follow isobaths and were steered offshore in the area between Cape Romain and Cape Fear. This veering of the flow may be partially due to the pronounced shoals around Cape Fear, which pose a natural barrier to the northward wind-driven flow on the shelf (see also the barotropic numerical simulation of wind-driven flow on the SAB by *Kourafalou et al.* [1984]). However, the rate and pathway of cross-shelf removal of coastal particles are primarily determined by the combined effect of stratification due to river discharge, wind-driven transports, and mixing due to wind and tides.

Figure 13 displays the final position of particles that were released from every model nodal point along approximately 200 km of coastline between 31°N and 33°N. The particles thus formed a line-type initial distribution that is marked between points A and B in Figure 13 at the coast (approximately between Savannah and Charleston). The trajectories were calculated within the near-surface and near-bottom model layers; no vertical

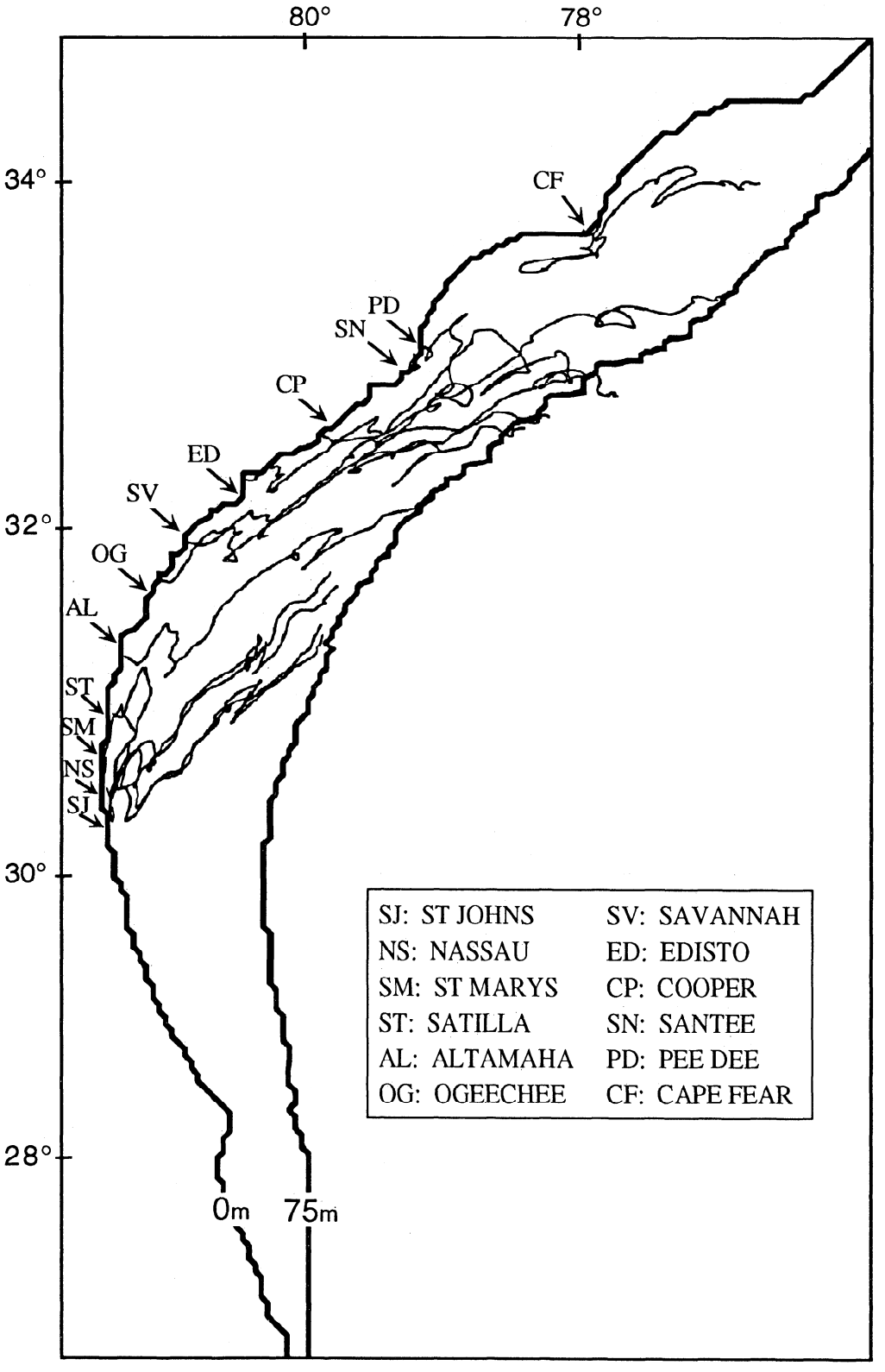

Figure 12. The 2-month (March-April 1984) trajectories of particles that were released at the mouth of the 12 major SAB rivers.

velocities were employed and therefore the particles remained within the initially specified range in the water column. The final location of each particle is marked with a circle or a cross for the 30-day and 60-day trajectory periods, respectively. It is obvious that the offshore, near-surface flow removed particles away from the discharge site, while onshore, near-bottom flow caused particle trapping. After 30 days of travel, only 40% of the initial particles remained in the inner shelf, while the rest were contained within the midshelf region. After 60 days of

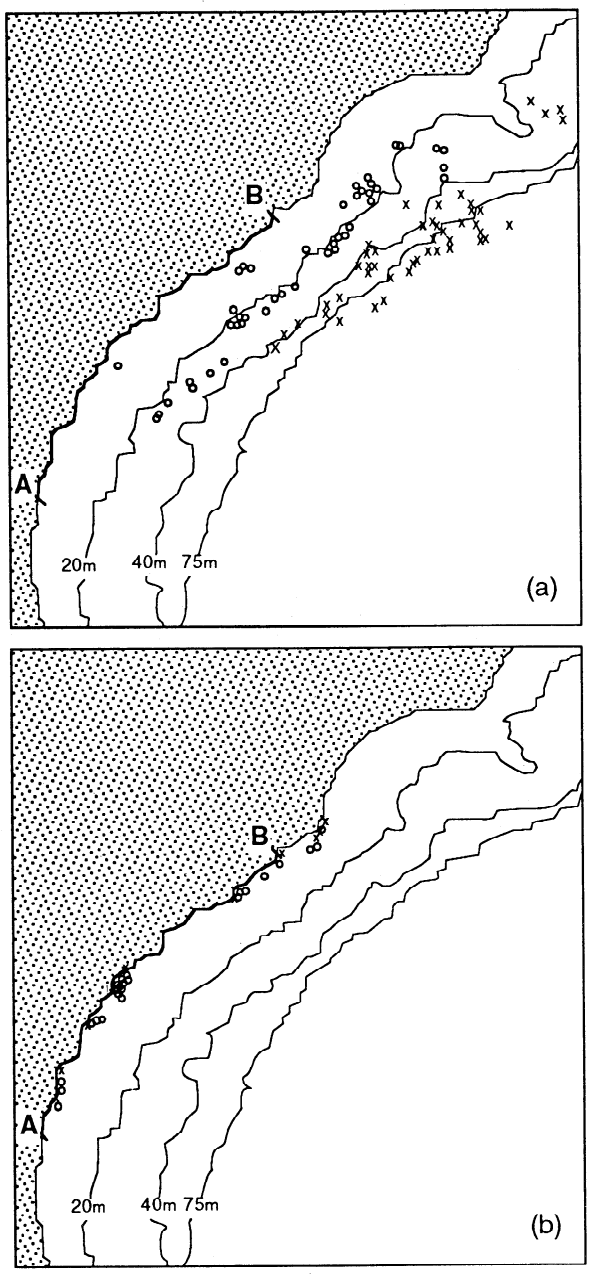

Figure 13. Final location of particles after a 1-month trajectory (March 1984, marked by circles) and after a 2-month trajectory (March-April 1984, marked by crosses). All particles were released along the coastal line labeled AB and traveled (a) near surface and (b) near bottom.

displacement all near-surface particles had been removed from the inner shelf, about half were concentrated in the outer shelf, and the other half had left the shelf region, presumably subject to the influence of the deep oceanic flow.

6. Concluding Remarks

We presented a comprehensive, three-dimensional model for the Southeast U.S. Continental Shelf (SAB) that includes detailed topography and accommodates the following three important circulation-forcing mechanisms: freshwater input from rivers, wind stress, and tides. The development and evolution of the nearshore low-salinity band that is generated through the river input and resides primarily within the inner shelf were studied during a realistic simulation of a typical spring season. The model resolved the inner shelf adequately and predicted realistic flow patterns on the shelf, including springtime transport of the riverine low-salinity waters and associated materials.

Our results suggest that the dominant mode of current variability over the shelf is the large-scale, wind-forced, barotropic response. The stratification conditions, however, determine the response of the shelf waters to the applied wind stress. For the shallow inner shelf region, downwind acceleration takes place mainly between rivers, i.e., outside the areas within the individual river plumes, where the buoyancy forcing is strong enough to overcome the wind stress. Consequently, very close to the runoff sites, there is a strong tendency for offshore flow, regardless of the wind conditions, with the tendency of establishing a buoyancy-driven southward current. When the coastal setup of sea level is enhanced by the wind (downwelling favorable), southward flow is dominant. During upwelling-favorable wind stress the southward turning of the baroclinic flow is retarded and often reversed at a rate that depends on the relative magnitude of the buoyancy and wind forcings. The flow adjustment periods are often characterized by opposite flows in the coastal and offshore shelf regions.

The most favorable conditions for an intense episode of offshore removal of coastal low-salinity waters include high river discharge, followed by a strong upwelling-favorable wind event. The path of removal of riverine waters can occasionally be confined within streamers directly related to the individual plumes of the strong SAB rivers, which then exhibit a point source behavior. However, the combination of conditions that is required for this response makes it a rather episodic type. At times when the inner shelf low-salinity band is well developed we occasionally observe the model formation of lenses of low-salinity water that travel toward the deeper shelf regions. Our findings suggest that these lenses are often short-lived and small, therefore difficult to detect in measurements. The mean path seems to originate in a nearshore region that behaves more like a "line source" of freshwater, and it follows the general direction of the mean springtime wind stress and the bathymetry, both of which favor the northeastward direction. On the mean, a continuous offshore removal of riverine water seems to take place.

We found that the cross-shore momentum balance was mainly between the Coriolis, pressure gradient, and wind stress terms. In the alongshore direction these terms were also important, with an additional contribution from the local acceleration and bottom stress terms.

We verified the hypothesis that during the spring season, riverine low-salinity water (and the plankton and material which it contains) is removed from the nearshore region to the part of the outer shelf that lies between approximately Savannah, Georgia (32°N), and Cape Fear, North Carolina (34°N). We inferred that this transport pattern is due to the prevailing northeastward direction of the wind stress during spring and the high river runoff which causes stratification of inner shelf waters as the plumes of individual rivers blend to form a low-salinity band. The SAB shelf exhibited

a remarkable self-cleaning mechanism during spring, as the simulated materials were removed away from the nearshore region in less than a month and reached as far as the outer shelf and off-shelf (beyond the shelf break) regions in about 2 months. These rates apply to particles that reside in the upper part of the water column, which includes materials that may be released near the surface, as well as materials that may rise from near-bottom discharge sites. However, particles that sink or otherwise reach the lower parts of the water column upon their release will generally remain close to the coast.

The study herein has not attempted an ecological analysis that would include biological, chemical, and geological considerations, such as the influence of freshwater discharge on marine life, the dilution rates of the important pollutants in the SAB, and the types of sediments that are being delivered. However, our findings on the response of the coastal ocean to sources of both momentum and buoyancy may serve as a guideline for future planning of experiments that would address ecological topics in detail.

Acknowledgments. Our appreciation is extended to Liz Williams for assistance with analysis of current meter data and to Jean Carpenter for drafting help. We greatly appreciate the computer time extended by NCAR for model runs on the CRAY Y-MP and the hydrographic land maps and river discharge data provided by the Water Resources Division of the U.S. Geological Survey. Funding for this work has been supplied by U. S. Department of Energy contract DE-FG05-85ER60355 and National Science Foundation grants OCE-88-12745 and OCE-89-11859.

References

Atkinson, L.P., T.N. Lee, J.O. Blanton, and W.S. Chandler, Climatology of the Southeastern United States Continental Shelf Waters, *J. Geophys. Res.*, *88*(C8), 4705-4718, 1983.

Bane, J.M., Initial observations of the surface structure and short-term variability of the seaward deflection of the Gulf Stream off Charleston, S.C., *J. Geophys. Res.*, *88*(C8), 4673-4684, 1983.

Blanton, J.O., and L.P. Atkinson, Transport and fate of river discharge on the continental shelf of the southeastern United States, *J. Geophys. Res.*, *88*(C8), 4730-4738, 1983.

Blumberg, A.F., and G.L. Mellor, Diagnostic and prognostic numerical circulation studies of the South Atlantic Bight, *J. Geophys. Res.*, *88*(C8), 4579-4592, 1983.

Flather, R.A., A tidal model of the northwest European continental shelf, *Mem. Soc. R. Sci. Liege*, Ser. 6, 10, 141-164, 1976.

Hansen, D.V., and M. Rattray, New dimensions in estuary classification, *Limnol. Oceanogr.*, *11*(3), 319-325, 1965.

Hsu, S.A., Models for estimating offshore winds from onshore meteorological measurements, *Boundary Layer Meteorol.*, *20*, 341-351, 1981.

Hsu, S.A., A mechanism for the increase of wind stress (drag) coefficient with wind speed over water surfaces: A parametric model, *J. Phys. Oceanogr.*, *16*, 144-150, 1986.

Kourafalou, V., J.D. Wang, T.N. Lee, and L.J. Pietrafesa, Modeling of winter circulation on the Southeast U.S. Continental Shelf, *Tech. Rep. 83009*, 97 pp., Univ. of Miami, Miami, Fla., 1983.

Kourafalou, V., J.D. Wang, and T.N. Lee, Circulation on the continental shelf of the southeastern United States, 3, Modeling the winter wind-driven flow, *J. Phys. Oceanogr.*, *14*, 1022-1031, 1984.

Kourafalou, V.H., Continental shelf response to freshwater input from rivers: A 3-D model study and applications, Ph.D. thesis, 218 pp., Univ. of Miami, Miami, Fla., 1993.

Kourafalou, V.H., L.-Y. Oey, J.D. Wang, and T.N. Lee, The fate of river discharge on the continental shelf, 1, Modeling the river plume and the inner shelf coastal current, *J. Geophys. Res.*, this issue.

Large, W.G., and S.Pond, Open ocean momentum flux measurements in moderate to strong winds, *J. Phys. Oceanogr.*, *11*, 324-336, 1981.

Lee, T.N., W.-J. Ho, V. Kourafalou, and J.D. Wang, Circulation on the continental shelf of the southeastern United States, 1, Subtidal response to wind and Gulf Stream forcing, *J. Phys. Oceanogr.*, *14*, 1001-1012, 1984.

Lorenzzetti, J.A., J.D. Wang, and T.N. Lee, Two-layer model of summer circulation on the Southeast U.S. Continental Shelf, *J. Phys. Oceanogr.*, *18*, 591-608, 1988.

McClain, C.R., J.A. Yoder, L.P. Atkinson, J.O. Blanton, T.N. Lee, J.J. Singer, and F.Muller-Karger, Variability of surface pigment concentrations in the South Atlantic Bight, *J. Geophys. Res.*, *93*(C9), 10,675-10,697, 1988.

Miller, J.L., Dynamics of Gulf Stream meanders and frontal eddies in the South Atlantic Bight, Ph.D. dissertation, 131 pp, Univ. of Miami, Miami, Fla., 1992.

Oey, L.Y., and P. Chen, A model simulation of circulation in the northeast Atlantic shelves and seas, *J. Geophys. Res.*, *97*(C12), 20,087-20,115, 1992.

Paffenhofer, G.-A., L.P. Atkinson, T.N. Lee, J.O. Blanton, B.K. Sherman, and T.B. Stewart, Variability of particulate matter and abundant zooplankton off the Southeastern United States during spring of 1984 and 1985, *Cont. Shelf Res.*, *14*(6), 629-654, 1994.

Pietrafesa, J.L., J.O. Blanton, J.D. Wang, V. Kourafalou, T.N. Lee, and K.A. Bush, The tidal regime in the South Atlantic Bight, in *Oceanography of the Southeastern U.S. Continental Shelf, Coastal Estuarine Stud. Ser.*, vol. 2, edited by L.P. Atkinson, D.W. Menzel, and K.A. Bush, pp. 63-76, AGU, Washington, D.C., 1985.

Schwiderski, E.W., On charting global ocean tides, *Rev. Geophys.*, *18*(1), 243-268, 1980.

Singer, J.J., L. Atkinson, J.O. Blanton, and J.A. Yoder, Cape Romain and the Charleston Bump: Historical and recent hydrographical observations, *J. Geophys. Res.*,*88*(C8), 4685-4698, 1983.

Wang, J.D., Real-time flow in unstratified shallow water. *J. Waterw. Port Coastal Ocean Div. Am. Soc. Civ. Eng.*, *104*(WW1), 53-68, 1978.

Wang, J.D., and J.J. Connor, Mathematical modeling of near coastal circulation, 272 pp., *Tech. Rep. 200*, R.M. Persons Lab., Dep. of Civ. Eng., Mass. Inst. of Technol., Cambridge, 1975.

Wang, J.D., V. Kourafalou, and T.N. Lee, Circulation on the continental shelf of the southeastern United States, 2, Model development and application to tidal flow, *J. Phys. Oceanogr.*, *14*, 1013-1021, 1984.

Wu, J., Wind stress coefficients over sea surface from sea breeze to hurricane, *J. Geophys. Res.*, *87*(C12), 9704-9706, 1982.

V. H. Kourafalou, Consiglio Nazionale delle Ricerche, Istituto per lo Studio delle Metodologie Geofisiche Ambientali, 770 Via Emilia Est Modena, 41100 Italy. (e-mail: villy@elektra.bo.cnr.it

T. N. Lee, Rosenstiel School of Marine and Atmospheric Science, University of Miami, Division of Meteorology and Physical Oceanography, Miami, FL 33149 (e-mail: tlee@rsmas.miami.edu)

L.-Y. Oey, Atmospheric and Oceanic Science Program, Princeton University, Sayre Hall, Forrestal Campus, Princeton, NJ 08544. (e-mail: lyo@kuroshio.princeton.edu)

J. D. Wang, Rosenstiel School of Marine and Atmospheric Science, University of Miami, Division of Applied Marine Physics, Miami, FL 33149 (e-mail: jwang@rsmas.miami.edu)

(Received October 13, 1994; revised June 2, 1995; accepted October 2, 1995.)